PEOPLE'S DEMOCRATIC REPUBLIC OF ALGERIA
الجمهورية الجزائرية الديمقراطية الشعبية
MINISTRY OF HIGHER EDUCATION AND SCIENTIFIC RESEARCH
وزارة التعليم العالي و البحث العلمي
UNIVERSITY OF BISKRA
جامعة محمد خيضر بسكرة

FACULTY OF SCIENCE AND TECHNOLOGIES
كلية العلوم و التكنولوجيا
DEPARTMENT OF MECHANICS
قسم الهندسة الميكانيكية

Master Thesis

Domain Sciences and Technologies
Field Mechanical Engineering
Option Construction

By:
Sabri Mohamed Sebti

Topic

Simulation Of Double Leading-Edge Slat On Airfoil Performance in Ansys fluent.

Defended Publicly in Front of the Jury Composed of

M_r.	A.BENCHABANE	PRESIDENT	USTB
M_r.	S,GUERBAAI	EXAMINER	USTB
M_r.	N.CHOUCHANE	SUPERVISOR	USTB

Academic Year 2023/2024

Acknowledgements

I would like to express my deepest gratitude to everyone who has supported and guided me throughout the course of this research.

First and foremost, I am profoundly grateful to my parents. Their unwavering support, encouragement, and belief in my abilities have been my greatest source of strength and motivation. Without their endless sacrifices and unconditional love, this journey would not have been possible. They have always stood by me, and I dedicate this work to them.

I would also like to extend my heartfelt thanks to my friends, whose encouragement and understanding have been invaluable. Their companionship and constant support have provided me with the balance and perspective needed during challenging times.

I am also deeply appreciative of the guidance and mentorship provided by my supervisor during my internship at Air Tassili. Their insights, support, and encouragement significantly contributed to my professional growth and the successful completion of this research.

Lastly, I would like to acknowledge the guidance and support of my teachers. Their expertise, mentorship, and dedication have played a crucial role in shaping my academic and research endeavors.

This thesis is a testament to the collective support and

encouragement of my family, friends, and teachers, to whom I am eternally grateful.

General Introduction

The aerodynamic performance of airfoils plays a crucial role in the design and efficiency of modern aircraft. among various aerodynamic devices, leading-edge slats are extensively utilized to enhance lift and delay stall, thereby improving the overall performance and safety of aircraft during takeoff and landing phases, this study focuses on the simulation and analysis of a 2d airfoil equipped with leading-edge slats, utilizing the computational fluid dynamics (cfd) software fluent. The primary objective of this research is to demonstrate the aerodynamic advantages of using two slats compared to a single slat configuration; by leveraging advanced simulation techniques, we aim to provide a comprehensive understanding of the flow characteristics

around the airfoil and quantify the performance improvements offered by our proposed dual- slat design.

In the course of this thesis, we will detail the methodology employed to model the airfoil and slat configurations, including the geometric setup, meshing strategies, and the selection of appropriate turbulence models. the simulation results will be meticulously

analyzed to compare lift, drag, and flow separation patterns between the single-slat and dual- slat configurations.

We will also compare the original airfoil to the airfoil with closed slat, this will give us more insight into our designee flaw and help us improve the geometry of the slats. Ultimately, this

research seeks to contribute valuable insights into the design optimization of airfoils with leading-edge slats, offering potential improvements in aircraft performance and efficiency, through rigorous cfd analysis, we aim to validate the superiority of our dual-slat design, paving the way for advancements in aerodynamic technology.

Table of Contents

Acknowledgements i

General Introduction iii

Table of Contents v

List of Figures ix

List of Tables xiii

I Generalities And Nomenclature 1

1 Introduction . . . 2

2 Airfoil Nomenclature [1] : . . . 2

2.1 The Mean Camber Line: . . . 3

2.2 The Leading and Trailing Edges: . . . 3

2.3 The Chord Line: . . . 4

2.4 Camber: . . . 4

2.5 The relative wind: . . . 4

2.6 The angle of attack α: . . . 5

2.7 The drag D: . . . 5

2.8 The lift L: . . . 5

2.9 The moment M: . . . 5

3 Lift, Drag, and Moment Coefficients: [1] . . . 5

3.1 Lift Coefficient (CL): . . . 5

3.2 Drag Coefficient (CD): . . . 6

3.3 Moment Coefficient (CM): . . . 6

3.4 Lift to Drag Ratio (CL/ CD): . . . 7

3.5 Angle of Attack (AOA): . . . 7

3.6 Stalls: . . . 8
4 Airflow Around an Airfoil [3]: . . . 9
4.1 Reynolds number: . . . 9
4.2 Boundary Layer Effects and Flow Separation [4]: . . . 10
4.3 The wake: . . . 11
5 Leading-edge slat: . . . 12
6 Conclusion: . . . 13

II Simulation Preparation From Workbench to Fluent 14

1 Introduction . . . 15
2 Workbench Configuration: . . . 15
2.1 No SLAT Configuration Workbench: . . . 15
2.2 One SLAT Configuration Workbench: . . . 16
2.3 Two SLAT Configuration Workbench: . . . 16
2.4 Closed SLAT Configuration Workbench: . . . 16
3 Airfoil Selection: . . . 17
4 Type of Mesh: [11] . . . 20
4.1 C-Mesh: . . . 20
4.2 O-Mesh: . . . 21
4.3 H-Mesh: . . . 21
4.4 Choosing the Right Mesh: . . . 22
5 Creating the geometry: . . . 23
5.1 Airfoil coordinate: . . . 23
5.2 The Far-field: . . . 25
5.3 TWO SLATs Configuration Geometry: . . . 25
5.4 ONE SLAT Configuration Geometry: . . . 27
5.5 Closed SLATs Configuration Geometry: . . . 28
6 The Meshing: [13] . . . 28
6.1 Boundary Layer Resolution and Y+: [4] . . . 30
6.1.1 Understanding Y+ . . . 30
6.1.2 Y+ Guidelines: . . . 31
6.2 Calculating our first cell distance: . . . 31
6.3 Implementing Boundary Layer Meshes: . . . 31
6.3.1 Inflation Layers: . . . 31
6.3.2 Parameters to define: . . . 32
6.3.3 Best Practices: . . . 32

7 The configurations: . . . 32
7.1 No SLAT configuration meshing: . . . 32
7.2 One and two SLATs configuration meshing: . . . 34
7.3 Closed SLATs configuration meshing: . . . 35
7.4 Inflation Parameters: . . . 36
8 Navier-Stokes Equations: . . . 37
8.1 Conservation of Mass (Continuity Equation) . . . 37
8.2 Conservation of Momentum (Navier-Stokes Equations): . . . 38
8.3 Conservation of Energy: . . . 39
9 Solver Configuration: [6] . . . 40
9.1 Type of solver: . . . 41
9.1.1 Pressure-based solver: . . . 41
9.1.2 Density-based solver: . . . 41
9.2 Choosing Between the two solvers: . . . 42
9.3 Velocity formulation: . . . 42
9.4 Time options: . . . 42
9.5 Turbulence model: . . . 42
9.6 Boundary condition: . . . 44
9.7 Reference value option: . . . 45
9.8 Materials selection: . . . 46
10 Solution methods: [6] . . . 47
10.1 Schemes type: . . . 48
10.1.1 SIMPLE and SIMPLEC scheme: . . . 48
10.1.2 Coupled scheme: . . . 48
10.1.3 PISO (Pressure-Implicit with Splitting of Operators): . . . 48
10.1.4 Choosing our scheme: . . . 48
10.2 Pseudo time method: . . . 50
10.3 Discretization schemes: . . . 51
11 Solution initialization: [6] . . . 51
12 Residuals monitoring: [6] . . . 51
13 Running the Calculation: . . . 52
14 Conclusion . . . 53

III Result exposition and discussion **55**

1 USA-35B Simulation results: 56
2 V-2Closed SLAT Configuration Results: 60
3 Comparison between Closed 2 SLAT and No SLAT Configuration: 61
4 Two SLATs Configuration Results: 63
5 1 SLOT Configuration Results: 67
6 Comparison between 1 SLAT and 2 SLAT Configuration: 68
7 Conclusion: 72

General Conclusion **75**

References **78**

List of Figures

I.1 Sketch of a wing and airfoil. [1] . . . 3

I.2 Airfoil nomenclature [1]. . . . 3

I.3 Sketch showing the definitions of lift, drag, moments, AOA, and relative wind [1]. . . . 4

I.4 Diagram of Lift Curve [8]. . . . 8

I.5 Critical angle of attack and stall [2]. . . . 8

I.6 boundary layer thickness [9]. . . . 11

I.7 Air flows around the ball [10]. . . . 12

I.8 Airfoil with leading edge slats or flaps. [3]. . . . 12

II.1 No SLAT Workbench Setup . . . 15

II.2 Two SLAT Workbench Setup. . . . 16

II.3 One SLAT Workbench Setup. . . . 17

II.4 Closed SLAT Workbench Setup. . . . 17

II.5 Scrappy by Make patey. . . . 18

II.6 Geometry over view from the database [5][6]. . . . 18

II.7 Cub Crafter SS. . . . 19

II.8 C-type pattern for a blunt leading-edge airfoil 20

II.9 O-type pattern for a blunt leading-edge airfoil. . . . 21

II.10 H-type pattern with boundary layer clustering around an airfoil. 22

II.11 Zoom in the trailing edge of the USA 35B [5]. 23
II.13 Enter Caption 24
II.12 Our USA-35B drawn in Solid-works. 24
II.14 Our finals Geometry in Design-modeler. 25
II.15 total over view of our finished geometry with 2 SLATs. 26
II.16 Zoom in the 2SLAT'S. 26
II.17 Clos up of the Airfoil with the 2 SLATs. 27
II.18 total over view of our finished geometry with 1 SLATs. 27
II.19 Closed up of the Airfoil with the 1 SLATs. 27
II.20 Clos up of the Airfoil with the closed SLATs. 28
II.21 Zoom in the 2 SLATs closed. 28
II.22 Boundary layer representation with Y+ [9] [12]. 31
II.23 Full view of the no slot Mesh. 33
II.24 Inlet named selection 33
II.25 Outlet named selection 33
II.26 Airfoil named selection 34
II.27 Two slots full mesh 34
II.28 zoom one the airfoil mesh for 2 SLATs 35
II.29 zoom in the 2 SLATs 35
II.30 zoom in the 1 SLATS 35
II.31 Closed SLATs airfoil Mesh 36
II.32 Closed SLATs top side zoom 36
II.33 Closed SLATs Bot side zoom 36
II.34 Inflation Details. 37
II.35 Fluent solver panel 41
II.36 Fluent Viscous model's panel 43

II.37 Fluent Dropdown boundary's conditions. 44
II.38 Fluent Velocity inlet Panel 45
II.39 Fluent Reference values 46
II.40 Fluent materials creation and editing panel 46
II.41 Fluent Solution methods panel 47
II.42 Fluent Residual monitors plan. 52
II.43 Fluent Calculation Startup panel 53

III.1 Chart for the Lift coefficient for AOA. 56
III.2 Chart for the Drag coefficient for AOA. 56
III.3 Chart for the Lift to Drag Coefficient for AOA. 58
III.7 The contour plots of velocity distribution at 15° 59
III.4 The contour plots of velocity distribution at 0° 59
III.5 The contour plots of velocity distribution at 5° 59
III.6 The contour plots of velocity distribution at 10° 59
III.8 The contour plots of velocity distribution at 20° 60
III.9 The contour plots of velocity distribution at 0° in closed SLAT. 61
III.10 The contour plots of velocity distribution at 10° in closed SLAT. 61
III.11 The contour plots of velocity distribution at 20° in closed SLAT. 61
III.12 Chart for the Lift coefficient for AOA in SLATs and no SLAT configuration. 62
III.13 Chart for the Lift to Drag Coefficient for AOA in SLATs and no SLAT configuration. 62
III.14 Chart for the Drag coefficient for AOA in SLATs and no SLATS configuration 63
III.15 The contour plots of velocity distribution in the Closed SLATs region. 63
III.16 Chart for the Lift to Drag coefficient for AOA in 2 SLATs. . . . 65

III.17The contour plots of pressure distribution in the Two SLATs region. 65

III.18The contour plots of pressure distribution in the Two SLATs region. 65

III.19The contour plots of velocity distribution in the One SLATs region. 68

III.20The contour plots of pressure distribution in the One SLATs region. 68

III.21Chart for the Lift to Drag Coefficient for AOA in SLATs configuration. 69

III.22The contour plots of velocity distribution at 20° in Two SLAT. . 71

III.23The contour plots of velocity distribution at 20° in One SLAT . 71

III.24The contour plots of velocity distribution at 25° in Two SLAT . 71

III.25The contour plots of velocity distribution at 25° in One SLAT . 71

III.26The contour plots of velocity distribution at 30° in Two SLAT . 72

III.27The contour plots of velocity distribution at 30° in One SLAT . 72

List of Tables

III.1 USA-35B Simulation results for each AOA. 57

III.2 Closed SLATs Simulation results for each AOA. 60

III.3 result comparison for USA-35B and Closed SLATs. 62

III.4 Two SLATs Simulation Lift to Drag for each AOA. 64

III.5 Two SLATs Simulation results for each AOA. 66

III.6 One SLATs Simulation Lift to Drag for each AOA. 67

III.7 One SLATs Simulation Lift and Drag for each AOA. 69

III.8 Result comparison for Two SLATs and One SLATs. 70

Chapter I

Generalities And Nomenclature

1 Introduction

An airfoil is a 2D vertical cut of a given wing or blade section and they are the heart of modern aerodynamics, crucial in the design and function of aircraft wings, helicopter blades, wind turbine blades, and various other aerodynamic surfaces. An airfoil's primary function is to generate lift, that enables flight by overcoming gravity. Its shape, characterized by a leading edge, trailing edge, chord line, camber, and thickness distribution, is designed to maximize aerodynamic efficiency.

In this chapter we will explore the terminology and both and airfoil and it functionating but also the idea behind high lift device how they affect an airfoil performance, we also discuss how aerodynamic lift is produced

When an airfoil is moved at a particular speed, it generates aerodynamic forces (lift and drag), Drag force acts in the opposite direction of motion while the force that is in the vertical direction provides lift. Lift Force is created by the difference in pressures on top and bottom surfaces. Air travels at the same speed across both the top and bottom of an airplane's wings if they have the same shape. When an airplane's wings have an airfoil shape, air travels slower over the top than at the bottom. As a result, wings can generate extra lift because of the increased airflow. The curved airfoil design directs air downwards, resulting in a faster flow of air and thus more speed. Lift is increased in an airplane by the velocity differences between the top and bottom parts of the wing.

2 Airfoil Nomenclature [1] :

Consider the wing of an airplane, the cross-sectional shape obtained by the intersection of the wing with the perpendicular plane is called an airfoil.

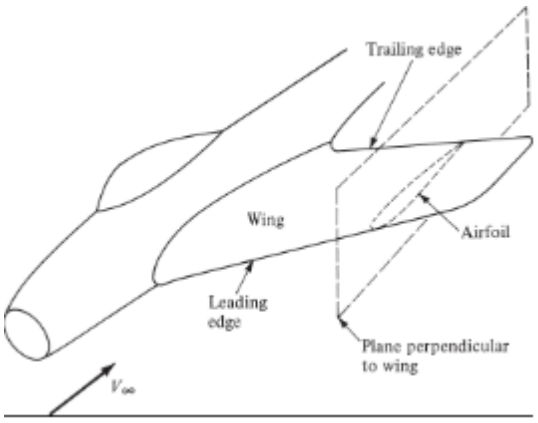

Figure I.1: Sketch of a wing and airfoil. [1]

Such an airfoil is sketched in Figure below, which illustrates some basic terminology:

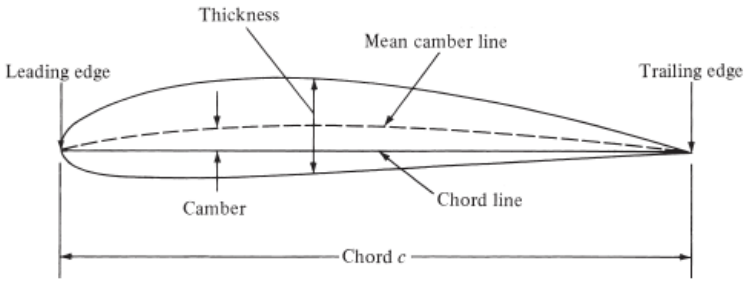

Figure I.2: Airfoil nomenclature [1].

2.1 The Mean Camber Line:

This is the primary design feature of an airfoil. It represents the locus of points halfway between the upper and lower surfaces, measured perpendicular to the mean camber line itself.

2.2 The Leading and Trailing Edges:

These are the most forward and rearward points of the mean camber line, respectively.

2.3 The Chord Line:

The straight line connecting the leading and trailing edges is known as the chord line. The distance from the leading edge to the trailing edge along this line is referred to as the chord of the airfoil.

2.4 Camber:

Camber is the maximum distance between the mean camber line and the chord line, measured perpendicular to the chord line.

The camber, the shape of the mean camber line, and, to a lesser extent, the thickness distribution of the airfoil fundamentally controls the lift and moment characteristics of the airfoil.

But this is not the end on airfoil nomenclature to see the rest we need to add a stream of air:

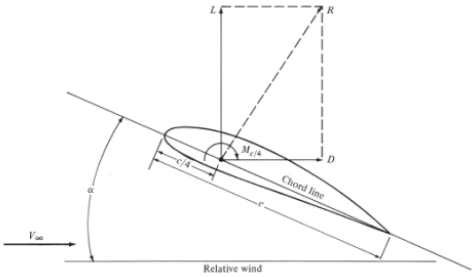

Figure I.3: Sketch showing the definitions of lift, drag, moments, AOA, and relative wind [1].

2.5 The relative wind:

Is the direction free-stream velocity V_∞ that is in itself the velocity of the air far upstream of the airfoil.

where:

- V is the variable or symbol,
- ∞ is the infinity symbol.

2.6 The angle of attack α:

Is the angle between the relative wind and the chord line, When air flows around an airfoil, it generates pressure and velocity variations in the surrounding flow field. This airflow exerts normal pressure forces and tangential shear forces on the surface of the airfoil. By integrating these forces over the airfoil's surface, we obtain the resultant aerodynamic force named R this force can be resolved into two forces, parallel and perpendicular to the relative wind.

2.7 The drag D:

is the component of the aerodynamic force parallel to the relative wind.

2.8 The lift L:

Is defined as the component of the aerodynamic force perpendicular to the relative wind.

2.9 The moment M:

Created by the surface pressure and shear stress distributions, this tends to rotate the wing.

3 Lift, Drag, and Moment Coefficients: [1]

The variations of L, D, and M depend at least on:

Free-stream velocity V_∞, Free-stream density V_∞, Size of the aerodynamic surface. For airplanes, we will use the wing area S to indicate size, Angle of attack α:, Shape of the airfoil, Viscosity coefficient μ_∞, Compressibility of the airflow, in our case it is 0 because we onlydeal with incompressible flow, from them we can get:

3.1 Lift Coefficient (CL):

The lift coefficient is a dimensionless number that quantifies the lift generated by an airfoil or wing relative to the fluid density and the flow

speed.
The lift coefficient C_L is defined by the following equation:

$$C_L = \frac{L}{\frac{1}{2}\rho V^2 S} \tag{I.1}$$

where:

- C_L: Lift coefficient,
- L: Lift force generated by the body,
- ρ: Density of the air,
- V: Velocity of the air relative to the body,
- S: Reference area of the body (typically wing area).

3.2 Drag Coefficient (CD):

The drag coefficient is a dimensionless number that quantifies the drag or resistance of an object.

The drag coefficient C_D is defined by the following equation:

$$C_D = \frac{D}{\frac{1}{2}\rho V^2 S} \tag{I.2}$$

where:

- C_D: Drag coefficient,
- D: Drag force acting on the body,
- ρ: Density of the air,
- V: Velocity of the air relative to the body,
- S: Reference area of the body (typically frontal area).

3.3 Moment Coefficient (CM):

The moment coefficient is a dimensionless number that quantifies the pitching moment generated by an airfoil.When neglecting the height difference between upper and lower side of an airfoil and keeping density

constant, if the velocity on the upper side of an airfoil exceeds the velocity on the lower side the pressure on the upper side must be lower than the pressure on the lower side of the airfoil. The moment coefficient C_M is defined by the following equation:

$$C_M = \frac{M}{\frac{1}{2}\rho V^2 Sc} \tag{I.3}$$

where:

- C_M: Moment coefficient,
- M: Moment or pitching moment,
- ρ: Density of the air,
- V: Velocity of the air relative to the body,
- S: Reference area of the body (typically wing area),
- c: Mean aerodynamic chord (MAC).

3.4 Lift to Drag Ratio (CL/ CD):

Because lift and drag are both aerodynamic forces, the ratio of lift to drag is an indication of the aerodynamic efficiency of the airplane.

3.5 Angle of Attack (AOA):

Us we said before The Angle of Attack is the angle at which relative wind meets an airfoil. It is the angle formed by the Chord of the airfoil and the direction of the relative wind or the vector representing the relative motion between the aircraft and the atmosphere. An increase in angle of attack results in an increase in both lift and induced drag, up to a point. Too high an angle of attack (usually around 17 degrees) and the airflow across the upper surface of the airfoil becomes detached, resulting in a loss of lift, otherwise known as a Stall.

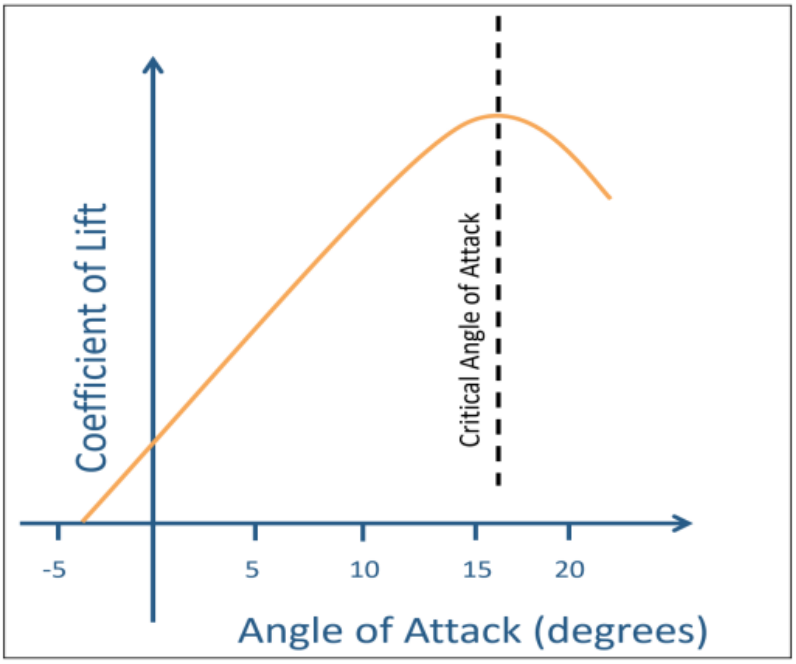

Figure I.4: Diagram of Lift Curve [8].

3.6 Stalls:

A stall is an aerodynamic condition that happens when the smooth airflow over an airplane's wings is interrupted, leading to a loss of lift. This occurs when the angle of attack (AOA) exceeds the wing's critical AOA. A stall can occur at any airspeed, attitude, or power setting.

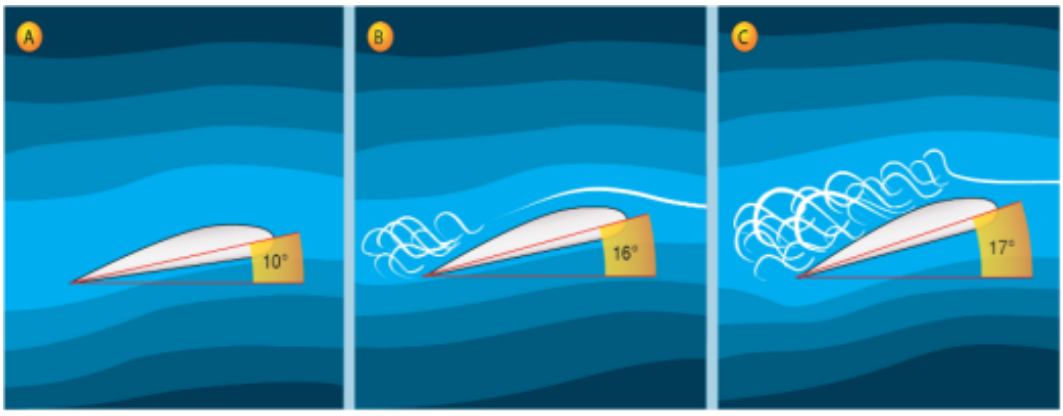

Figure I.5: Critical angle of attack and stall [2].

4 Airflow Around an Airfoil [3]:

The airflow around an airfoil is a critical aspect of aerodynamics, influencing the performance and efficiency of aircraft. As air approaches an airfoil, it splits into two streams that flow over and under the wing. The upper surface of the airfoil typically has a curved shape that causes the airflow to accelerate, reducing pressure according to Bernoulli's principle. This acceleration is essential for generating lift, a force that opposes gravity and allows the aircraft to rise. On the lower surface, the airflow moves more slowly, resulting in higher pressure.

The interaction between these two airflow streams creates a pressure differential, with lower pressure on the upper surface and higher pressure on the lower surface. This differential generates lift. The airflow reattaches at the trailing edge of the airfoil, where the pressure and velocity differences between the upper and lower surfaces are reconciled. The behavior of airflow near the surface of the airfoil is described by the boundary layer, a thin region where viscous forces are significant. Within this boundary layer, the air's velocity changes from zero at the surface (due to the no-slip condition) to the free-stream velocity outside the boundary layer.

4.1 Reynolds number:

As an object travels through the atmosphere, it disturbs the surrounding gas molecules, causing them to flow around the object. This interaction generates aerodynamic forces between the object and the gas. The magnitude of these forces depends on several factors, including the object's shape, speed, and the mass of the gas it encounters. Additionally, two crucial properties of the gas that are the viscosity and compressibility also influence the forces. If two experiments have the same values for the similarity parameters, then the relative importance of the forces are being correctly modeled; this mean if we have 2 airfoils of the same shape but at different scale, we can modify the velocity to

get the same Reynolds number and that will give us the same Lift, Drag, and Moment Coefficients.

There is different method of calculating the Reynolds number we will see them in later chapter.

4.2 Boundary Layer Effects and Flow Separation [4]:

When air moves over the surface of the airfoil the stability of the flow is influenced by the course of the airfoil as well as whether the flow is in the laminar or turbulent flow regime. The latter is predicted by the Reynolds number.L is the chord length of the airfoil and ν is the kinematic viscosity of the air,

"The Reynolds number is the ratio between inertial and viscous forces. The transition from laminar to turbulent flow occurs at approximately Re=500,000 for a smooth flat" The Reynolds number Re is defined by the following equation:

$$Re = \frac{V \cdot L}{\nu} \tag{I.4}$$

where:

- Re: Reynolds number,
- V: Velocity of the fluid,
- L: Characteristic length (such as diameter for a pipe or chord length for an airfoil),
- ν: Kinematic viscosity of the fluid.

The boundary layer is a thin region adjacent to a solid surface where viscous forces dominate the flow characteristics. Within this layer, the velocity of the fluid starts at zero at the surface due to the no-slip condition and gradually increases in the direction normal to the surface, eventually reaching 99% of the freestream velocity at the boundary layer's outer edge. This gradual velocity change defines the laminar boundary layer, where the flow is smooth and orderly. As the fluid

travels further downstream, the boundary layer thickness increases, and at a certain distance from the leading edge, it may transition to a turbulent state. This transition occurs when the viscous forces can no longer suppress the disturbances in the flow, resulting in a chaotic flow field characterized by irregular velocity fluctuations, vorticity, these phenomena greatly affect the Drag.

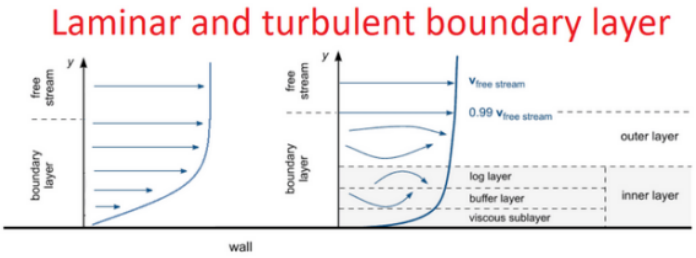

Figure I.6: boundary layer thickness [9].

4.3 The wake:

The wake, the region of disturbed airflow downstream of an airfoil, significantly impacts both the airfoil and overall aircraft performance. One major effect is the increase in drag, which includes both pressures drag (form drag) and induced drag. The turbulence and vortices within the wake contribute to higher energy losses, leading to elevated drag levels. This drag increase reduces the overall efficiency of the aircraft, requiring more power to maintain the same speed and resulting in higher fuel consumption.

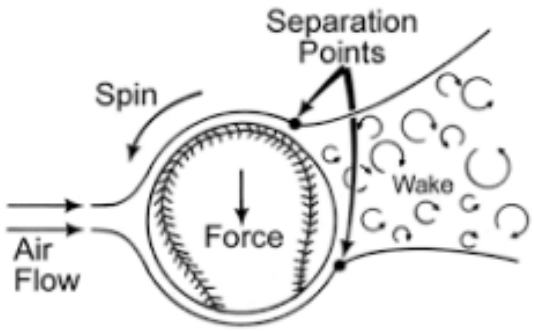

Figure I.7: Air flows around the ball [10].

5 Leading-edge slat:

A slat is an aerodynamic surface located on the leading edge of a fixed-wing aircraft's wing. When not in use, the slat lies flush with the wing. It deploys by sliding forward, creating a slot between the wing and the slat. This slot allows air from below the slat to flow through, replacing the boundary layer that has lost kinetic energy due to skin friction drag after traveling at high speed around the leading edge. By deploying slats, the wing can operate at a higher angle of attack before stalling, enabling the aircraft to fly at slower speeds and take off and land in shorter distances. Slats are particularly useful during takeoff, landing, and low- speed maneuvers that approach stall conditions. During normal flight, slats are retracted to minimize drag.

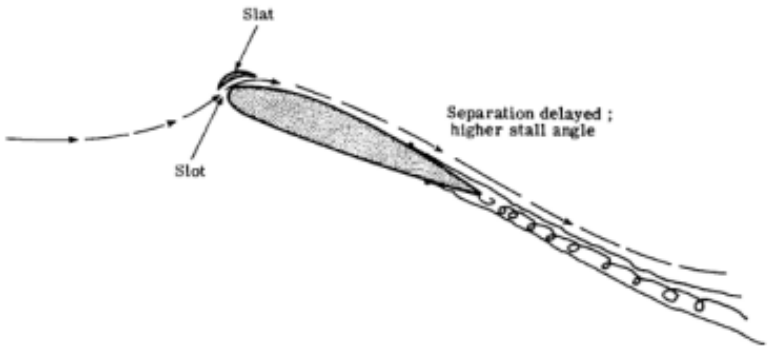

Figure I.8: Airfoil with leading edge slats or flaps. [3].

6 Conclusion:

Understanding the intricacies of airfoil design and airflow dynamics is fundamental to modern aerodynamics. The airfoil, with its specialized shape characterized by the leading edge, trailing edge, chord line, camber, and thickness distribution, is pivotal in the generation of lift, enabling flight and various aerodynamic applications. By delving into the terminology and functioning of airfoils, we have seen how their shape and movement through the air produce aerodynamic forces, particularly lift and drag. The lift force, essential for flight, is created by pressure differences across the airfoil's surfaces, a result of the air traveling at different speeds over the top and bottom surfaces.

Chapter II

Simulation Preparation From Workbench to Fluent

1 Introduction

In this chapter, we will detail our workbench setup, including the time required to complete each configuration. This transparency allows readers to understand how the setup can significantly impact calculation times and provides an opportunity to evaluate our organization. Additionally, we will present the initial stages of our simulation: the geometry preparation and the meshing of our chosen airfoil. We will begin by introducing the selected airfoil and explaining our reasons for this choice. Next, we will delve into the geometry creation, which involves preparing the CAD file to be exported to the meshing program. This file includes the airfoil, surface separations, and line bodies to ensure better-controlled meshing. Finally, we will showcase the resulting mesh and discuss the steps taken to create it.

2 Workbench Configuration:

2.1 No SLAT Configuration Workbench:

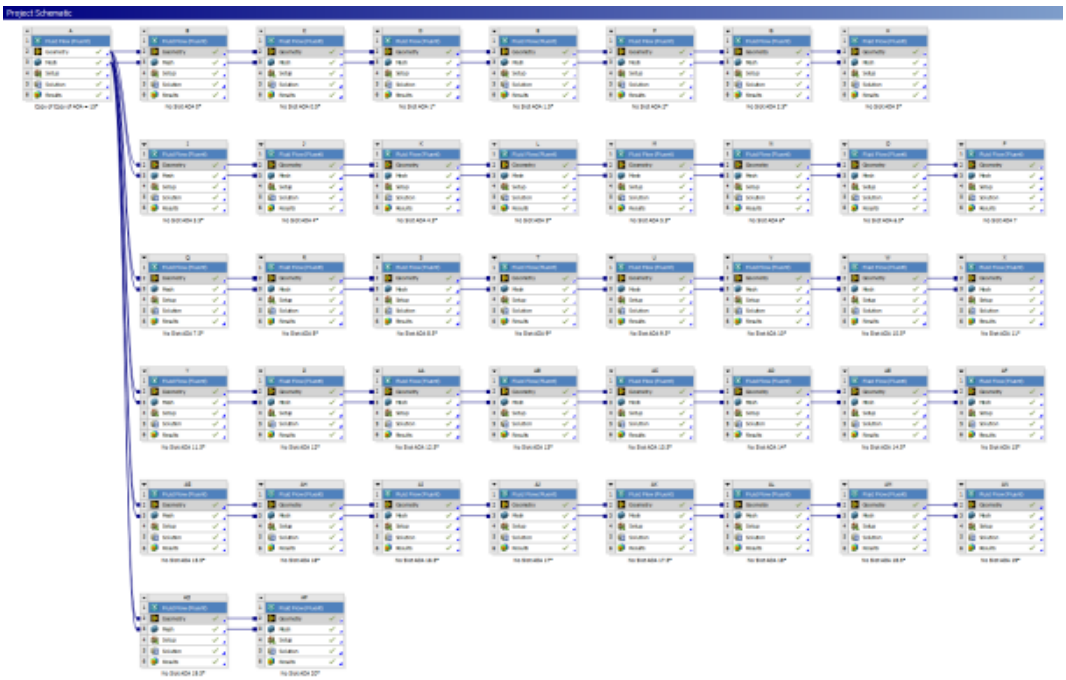

Figure II.1: No SLAT Workbench Setup

For this configuration we calculated the results from 0° to 20° with a 0.5° interval, this case took close to 144h of calculi time to finish.

2.2 One SLAT Configuration Workbench:

Since the Slot are used at high AOA, we will simulate our slot from 20° to 30° of AOA that is because a normal USA-35B airfoil stall around 19° thus we don't even need to compare our SLATs configuration to the airfoil performance, we will be working with a 0.25° intervale, this set up took 122H to finish.

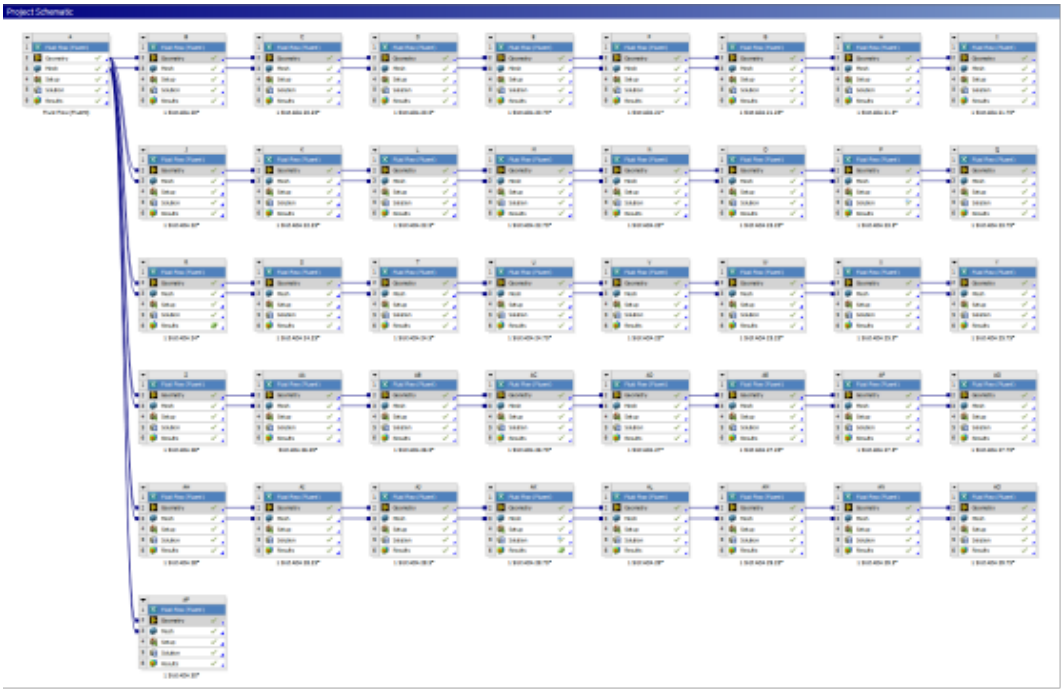

Figure II.2: Two SLAT Workbench Setup.

2.3 Two SLAT Configuration Workbench:

Same us the one slot configuration and took around the same time that is 122h to finish calculating.

2.4 Closed SLAT Configuration Workbench:

For these configurations we don't need to mush detail, for we will only use it to learn more about our design and it effect on airfoil at cruising

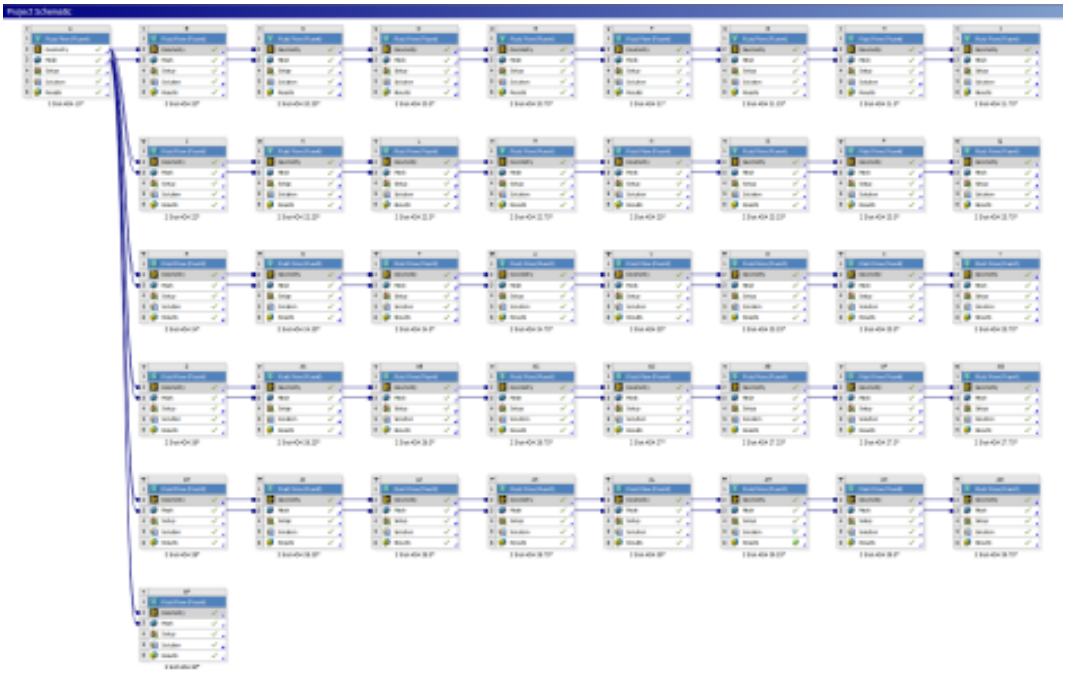

Figure II.3: One SLAT Workbench Setup.

position, but despite that this configuration still took 100h to calculate the results.

Figure II.4: Closed SLAT Workbench Setup.

3 Airfoil Selection:

When selecting our base geometry to start designing our leading-edge SLATs we first select our Airfoil and what is better to start our selection then the Airplane that first used the 2 SLOT configuration that is the

Scrappy From Mike Patey, but the Spec of this plane are kept secret and the inventor has not made them public yet so we don't know what is the airfoil used on it, but we know that the Scrappy is a modified CUBCRAFTER plane of the name Cub Crafter SS this particular plane did publish its airfoil name that is the : USA-35B MOD.

Figure II.5: Scrappy by Make patey.

Note: MOD stand for modified.

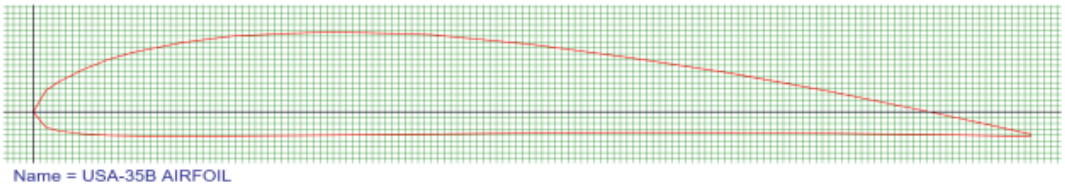

Figure II.6: Geometry over view from the database [5][6].

The USA-35B is renowned for its excellent performance characteristics that cater to the demands of light aircraft and bush planes. One of the primary advantages of the USA 35B airfoil is its outstanding lift-to-drag ratio, which significantly enhances the aircraft's efficiency. This airfoil is designed to provide high lift at relatively low speeds, making it ideal for short takeoff and landing (STOL) capabilities. This

is particularly beneficial for bush planes that operate on rough and unprepared airstrips. Additionally, the USA 35B airfoil contributes to the aircraft's stability and control, both critical factors for low-speed maneuvering and precision flying. The design also supports a broad range of flight conditions, offering versatility whether flying at higher altitudes or in varying weather conditions.

Figure II.7: Cub Crafter SS.

Now that we have the airfoil, we need to choose a size and for that we will keep the Chord length of the Cube Crafter SS, although the manufacturer of the plane did not specify it, they did give us the Wingspan and Wing Area that are 10.44m and 15.97m2, from there we calculate a chord length of approximately 1.53m. One of the positive of the Cub crafters is they are prebuilt and shipped, that give a chance for any one on the American soil to take their cub Crafter and modified it to use the SLATS that we designed and put it in wind tunnel to get experimental Data to improve it, in fact that where the Scrappy come from; the starting platform is a Cub EX prototype.

4 Type of Mesh: [11]

In Computational Fluid Dynamics (CFD), the type of mesh used significantly influences the accuracy and efficiency of simulations. Among the various mesh types, C- mesh, O-mesh, and H-mesh are commonly used, each offering unique characteristics and advantages tailored to different aerodynamic applications, the reason why we are selecting the type of mesh now is because the it is part of the geometry process and not the meshing process

4.1 C-Mesh:

A C-mesh is characterized by its C-shaped grid pattern that wraps around the airfoil. This mesh type is particularly effective for airfoil simulations because it provides high resolution in critical regions, such as the leading and trailing edges, while extending the farfield boundary to minimize its influence on the simulation. The C-mesh captures detailed flow patterns around the airfoil and ensures that the boundary layer is well-resolved, which is crucial for accurate drag and lift calculations. Its structure allows for a smooth transition from fine mesh near the airfoil surface to coarser mesh farther away, optimizing computational efficiency.

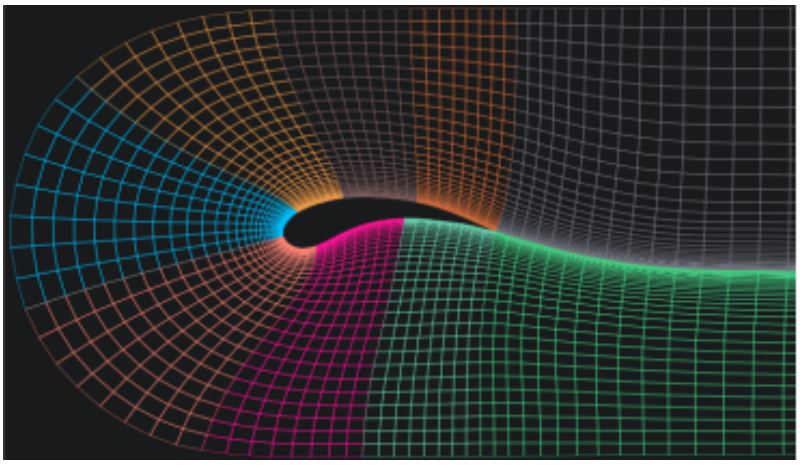

Figure II.8: C-type pattern for a blunt leading-edge airfoil .

4.2 O-Mesh:

The O-mesh features an O-shaped grid that encircles the airfoil or object in a concentric pattern. This type of mesh is advantageous for its ability to provide uniform grid spacing around the entire object, which helps in capturing symmetric flow features accurately. O-meshes are particularly useful for simulating rotational or axisymmetric flows and are often used in turbomachinery applications. The consistent grid structure around the object ensures that the boundary layer is uniformly resolved.

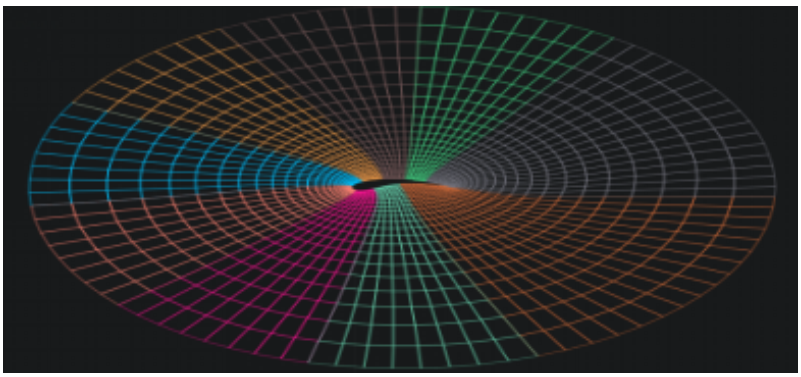

Figure II.9: O-type pattern for a blunt leading-edge airfoil.

4.3 H-Mesh:

H-meshes are characterized by their H-shaped grid pattern, where the grid lines are aligned in a Cartesian coordinate system, creating a more structured grid. This type of mesh is typically used for objects with sharp corners or flat surfaces, such as wings or flat plates. The H-mesh allows for easy grid generation and is computationally efficient for simple geometries. However, it may require additional refinement and careful alignment near curved surfaces or edges to ensure accurate flow resolution. The H-mesh is suitable for simulations where the flow features are predominantly aligned with the coordinate directions.

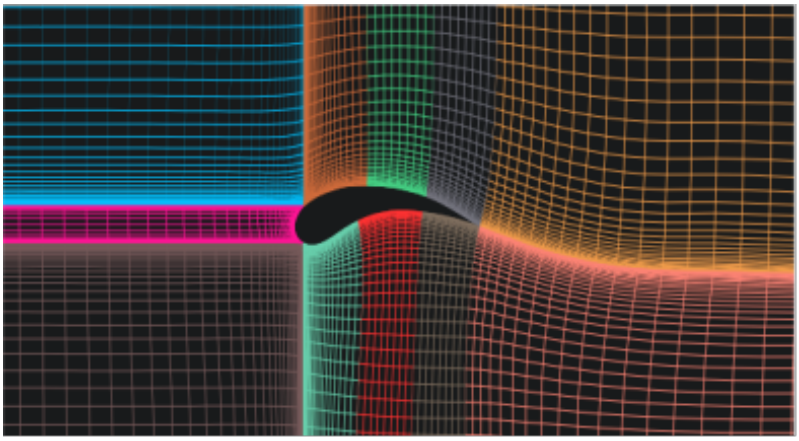

Figure II.10: H-type pattern with boundary layer clustering around an airfoil.

4.4 Choosing the Right Mesh:

To choose the proper mesh we need to take in consideration 2 fact about our airfoil:

- Our Airfoil in not symmetric.
- The flow features are Not aligned with the coordinate directions since we will study different Angle of attack.

The first point eliminates the O-Mesh type because it is best suited for symmetrical airfoil while the second point eliminate the H-Mesh type because it is best suited for simulations where the flow features are predominantly aligned with the coordinate directions if we wanted to use this Mesh we would need to create a different mesh for each angle of attack. That leave us with C-Mesh, the C-Mesh is the correct choice due to its exceptional ability to capture detailed flow patterns around complex geometries such as airfoils. The C- shaped grid pattern of the C-mesh wraps around the airfoil, providing high resolution in critical regions like the leading and trailing edges while minimizing the influence of the far-field boundary. This ensures accurate drag and lift calculations, essential for our analysis. Furthermore, NASA frequently employs C-meshes in its simulations of non-symmetrical airfoils, underscoring their effectiveness in handling the intricate flow

dynamics associated with these shapes. By utilizing a C-mesh, we align our methodology with best practices in aerospace research, ensuring robust and precise simulation results.
We previously said the far-field boundary need to be at minimum of 10 Chord length and mean for us 10x1530 that equals 15300mm.

5 Creating the geometry:

Downloading the CSV file of coordinates from the data base. Using the file, we create a Curve the follow the coordinate on it. We export our SLDPRT file to DesignModeler in Ansys to create our FarField and separation to better control our Meshing process. We Export our geometry to Ansys Meshing.

5.1 Airfoil coordinate:

It took us many days to realize that there are 2 problems with the database coordinate:

The coordinate is not at 0 Degre angle of attack that mean that we need to rotate our airfoil intel our camber line is horizontal.

Our Airfoil has an unclosed trailing edge that we need to alter so that the airfoil closes with a sharp trailing edge.

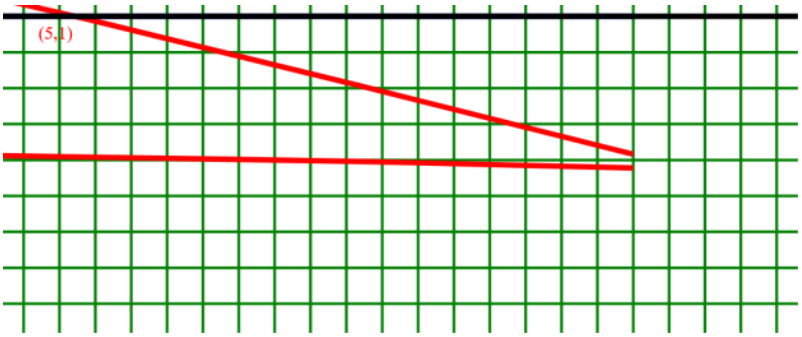

Figure II.11: Zoom in the trailing edge of the USA 35B [5].

After many try, we found that a using the coordinate of the airfoil with a 1513mm chord length and extended the 2 spline we get a perfect

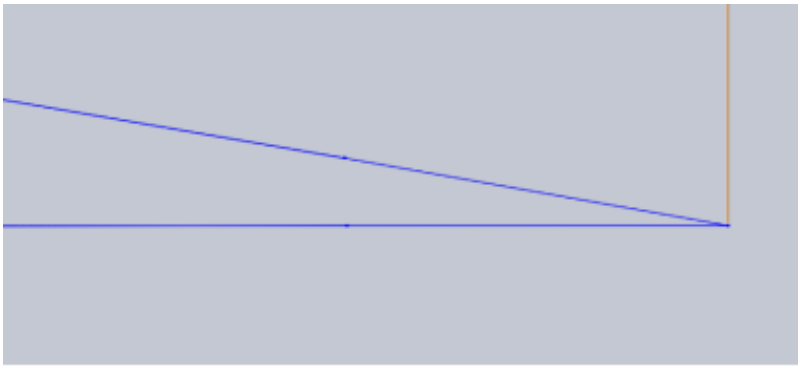

Figure II.13: Enter Caption

airfoil of a 1530 like we need it to be.

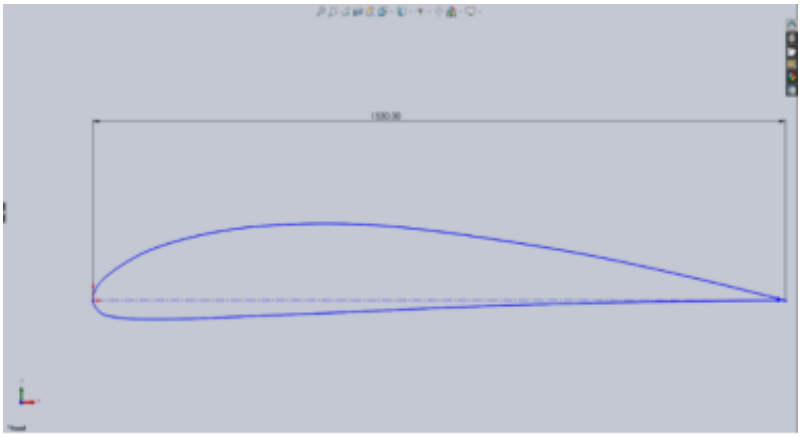

Figure II.12: Our USA-35B drawn in Solid-works.

When zooming on the trailing edge we can see our modification to make it Sharpe, we can also see that the 2 lines are Tangential to their respective Spline. Now our airfoil is ready we can export it to design modeler where we create our C Mesh form, this will be a 2D simulation so we will create a surface to be meshed with the airfoil been cut out of the From, that is because the airfoil will be considered us wall, for contrary to a static analysis in CFD we don't simulate the Structure rather we simulate the Fluid around it.

5.2 The Far-field:

This our finale geometry for this configuration, when creating your geometry for the Mesher we need to remember to add division and line body that will help us better controlee our meshing, for this reason we create 6 zone in our mesh this zone will help us better structure our mesh and keep a good quality.

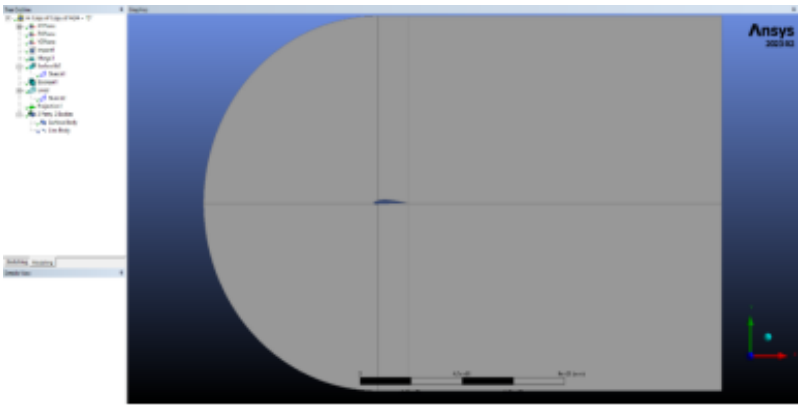

Figure II.14: Our finals Geometry in Design-modeler.

5.3 TWO SLATs Configuration Geometry:

The hardest part of this thesis was the design of the Leading-edge SLATs, that because all of the currently used models doesn't even publish their geometry never mind the methods of designing them.

That mean that we have to not only create our own SLATs we also need to develop our own methods of design, for this this we used a mix of creativity and reverse engineering the parameter that this company used to create their SLATs, for this reason only the finals result will be given, for our method still need mush refining before publishing.
All configuration will use a C mesh but the farfield boundary will change in X axes; after further testing we reduced the distance in this Axes to 10m from 15m without affecting the result, we went with this change to reduce the number of elements.

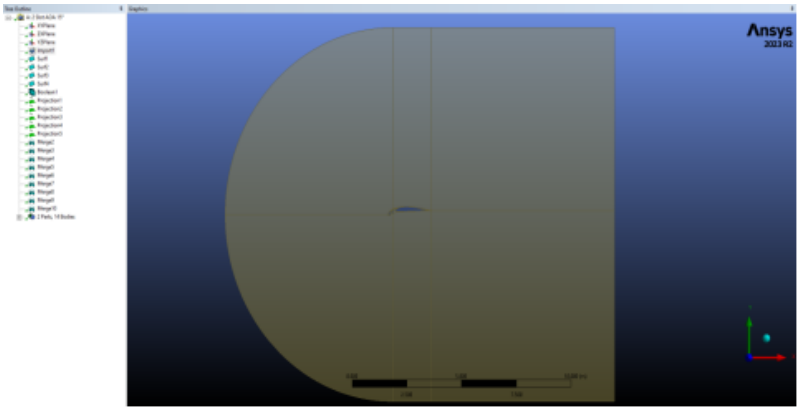

Figure II.15: total over view of our finished geometry with 2 SLATs.

The second change we make is to create 4 new zone to help us keep our mesh structured 3 of this are an offset of the airfoil and the SLATs profile these 3 zones will help create our inflation layer around the profile to properly resolve the boundary layer:

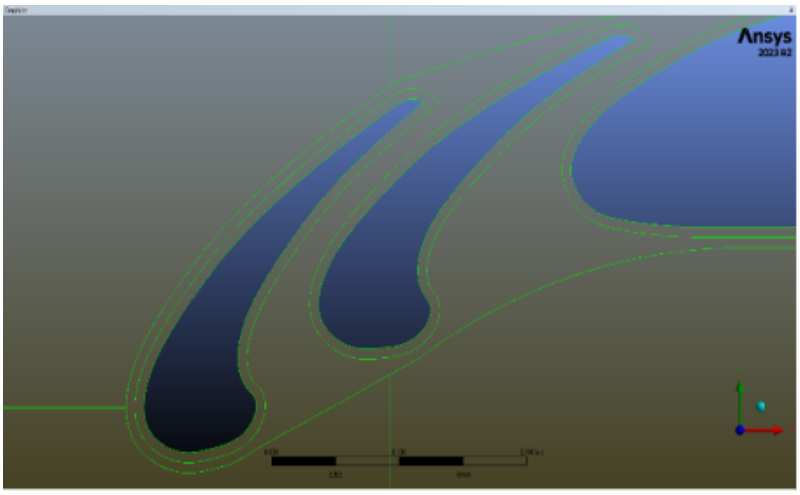

Figure II.16: Zoom in the 2SLAT'S.

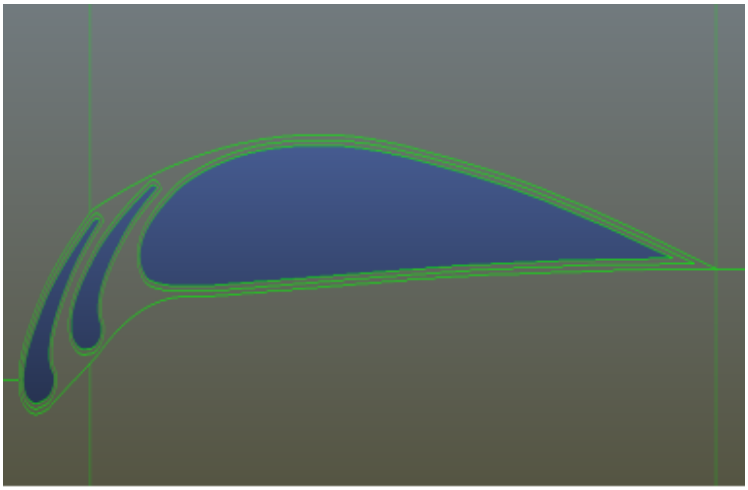

Figure II.17: Clos up of the Airfoil with the 2 SLATs.

and the for the zone is one that encompasses all of them:

5.4 ONE SLAT Configuration Geometry:

This configuration geometry follows the same principal then the first except that it only has 1 slot thus minus 1 zone in all:

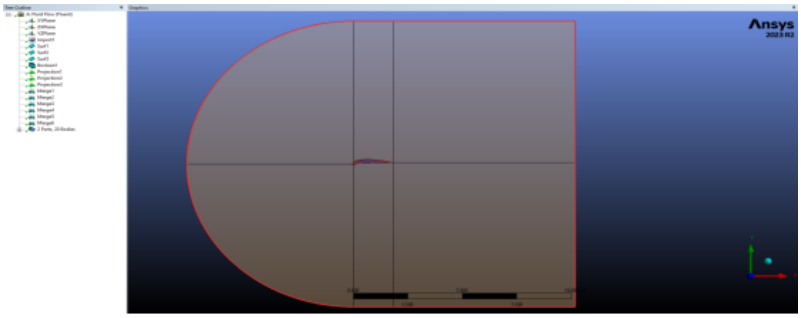

Figure II.18: total over view of our finished geometry with 1 SLATs.

A more zoomed in figure show there is only 1 SLAT:

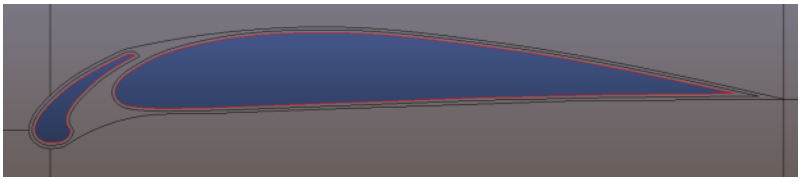

Figure II.19: Closed up of the Airfoil with the 1 SLATs.

5.5 Closed SLATs Configuration Geometry:

This configuration follows the same principal then the first no slat configuration with a change in the SLATs zone, but also, we need to smooth our geometry and rounded up the point of contact between the tips of the SLATs and the airfoil because they formed a too sharp of an angle that make it impossible to create an inflation layer.

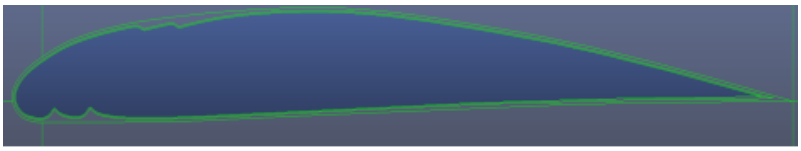

Figure II.20: Clos up of the Airfoil with the closed SLATs.

We added 2 contours to our airfoil for 2 reasons, the first contour is to control the inflation layer better, the second contour is because of the 2 dips caused by the SLATs; the big problem with them is that they need a bigger element count to properly represent the curvature, but also because without the separation they would cause the mesh to deform totally making a structured mesh impossible.

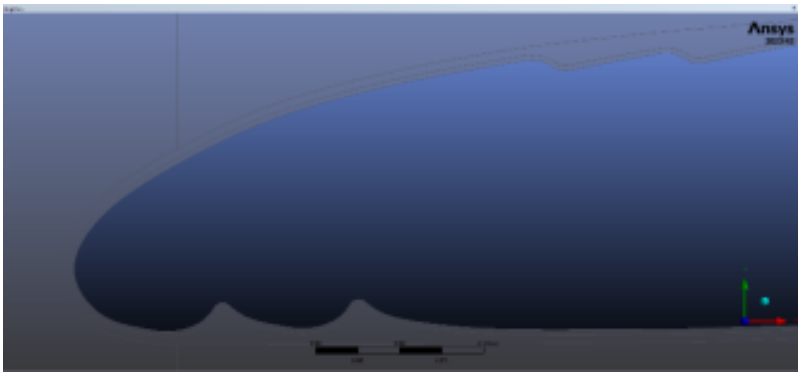

Figure II.21: Zoom in the 2 SLATs closed.

6 The Meshing: [13]

In computational fluid dynamics (CFD), the quality of the mesh is a decisive factor in the accuracy of simulation results, especially when analyzing airfoils. This chapter is dedicated to the creation of a

structured C-mesh for airfoil analysis, underscoring the importance of high-quality meshing and the incorporation of inflation layers.

The structured C-mesh is particularly advantageous for airfoil simulations due to its ability to conform closely to the airfoil's geometry while extending efficiently into the wake region. This type of mesh ensures a smooth and continuous grid, which is crucial for accurately capturing the flow patterns around the airfoil.

One of the critical areas in airfoil analysis is the boundary layer, the thin region close to the airfoil surface where the effects of viscosity are significant. Accurately resolving this region is essential for predicting key aerodynamic phenomena such as lift, drag, and flow separation. Inflation layers, which are finely spaced mesh layers near the airfoil surface, are vital for capturing the steep gradients in velocity and pressure within the boundary layer.

This chapter will guide you through the process of creating a structured C-mesh for airfoil analysis, from geometry preparation and mesh generation to the strategic implementation of inflation layers. Practical tips and techniques will be provided to help you avoid common pitfalls and ensure that your mesh supports accurate and reliable CFD simulations. By the end of this section, you will have a solid understanding of how to create high-quality meshes that enhance the precision of your airfoil analyses.

We have 4 configurations that mean we have 4 mesh to do we will explain the property of each one and the limitation we face for each one and the trad we have to take to keep our mesh us structured us possible around complicated regions. But before that we need to first know about the concept of Y+ and the resolution of the Boundary layer.

6.1 Boundary Layer Resolution and Y+: [4]

Effective boundary layer resolution is crucial for accurate CFD simulations, particularly when dealing with aerodynamic surfaces like airfoils. The boundary layer is the thin region near the surface of the airfoil where viscous effects are significant, and capturing its behavior accurately is essential for predicting aerodynamic performance such as lift, drag, and flow separation. One of the key parameters in boundary layer resolution is Y+, a dimensionless wall distance that indicates how well the mesh resolves the viscous sublayer.

6.1.1 Understanding Y+

Y+ is defined as:

$$Y^+ = \frac{y u_\tau}{\nu} \tag{II.1}$$

where:

- Y^+ is the dimensionless wall distance (wall coordinate)
- y is the distance from the wall
- u_τ is the friction velocity .
- ν is the kinematic viscosity

The value of Y+ determines which part of the boundary layer the first cell center resides in, guiding the meshing strategy to ensure proper boundary layer resolution.

$$u_\tau = \sqrt{\frac{\tau_m}{\rho}} \tag{II.2}$$

where:

- u_τ is the friction velocity
- τ_m is the wall shear stress
- ρ is the fluid density

6.1.2 Y+ Guidelines:

- **Low** Y^+ $(Y^+ < 1)$: Required for resolving the viscous sublayer directly, often necessary for high-fidelity simulations using Direct Numerical Simulation (DNS) or wall-resolved Large Eddy Simulation (LES). This involves extremely fine mesh near the wall.
- **Moderate** Y^+ $(1 < Y^+ < 5)$: Adequate for most Reynolds-Averaged Navier-Stokes (RANS) simulations with low-Re turbulence models, where the viscous sublayer is resolved accurately.
- **High** Y^+ $(30 < Y^+ < 300)$: Suitable for wall-function approaches in RANS simulations, where the near-wall treatment is modeled rather than resolved. This allows for coarser meshes near the wall.

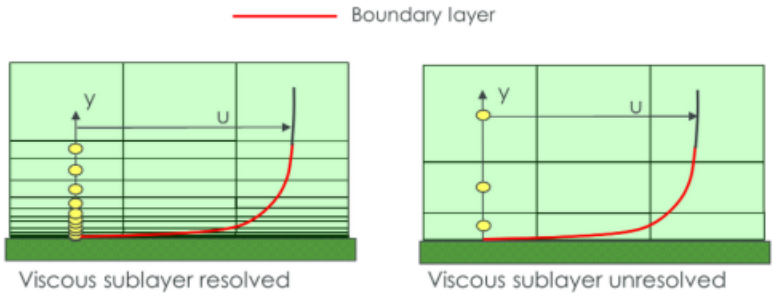

Figure II.22: Boundary layer representation with Y+ [9] [12].

6.2 Calculating our first cell distance:

We will be going with a Y+ = 1 for a free stream velocity of U=20m/s despite simulating our airfoil at 10m/s that is because the SLATs would energize the air and increase it speed so we go ahead and prepare for it this give us a y=0.018mm

6.3 Implementing Boundary Layer Meshes:

6.3.1 Inflation Layers:

Inflation layers are a series of finely spaced mesh layers near the wall, progressively increasing in thickness. These layers ensure that the steep

velocity and pressure gradients within the boundary layer are captured.

6.3.2 Parameters to define:

- **First Layer Thickness**: Determines the thickness of the first cell layer adjacent to the wall. It should be chosen to achieve the desired Y^+ value.
- **Growth Rate**: Controls how rapidly the thickness of subsequent layers increases. Typical values range from 1.1 to 1.3.
- **Number of Layers**: Specifies the total number of inflation layers to adequately resolve the boundary layer.

6.3.3 Best Practices:

- **Smooth Transition**: Ensure a smooth transition between the inflation layers and the core mesh to avoid numerical instabilities.
- **Mesh Quality**: Maintain high-quality elements in the inflation region, avoiding skewed or distorted cells.
- **Iterative Refinement**: Perform mesh convergence studies to refine the mesh iteratively, ensuring that results are independent of the mesh resolution.

7 The configurations:

7.1 No SLAT configuration meshing:

To control our mush and make structure we will using the edge sizing option with a bias factor to create our inflation layer and also concentrate our elements around the airfoil.

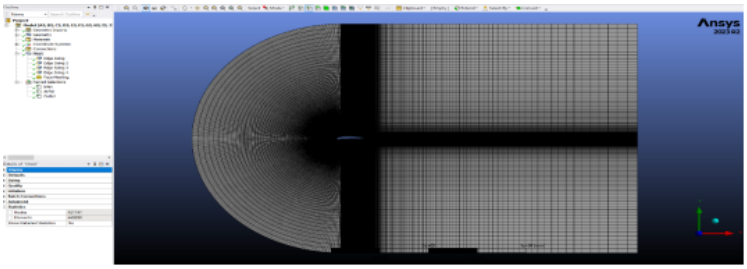

Figure II.23: Full view of the no slot Mesh.

Something to not the boundary condition creation happens in the meshing rather then in fluent and it is done by creating named selections that represent the boundary condition the inlet and outlet are the same in all configuration:

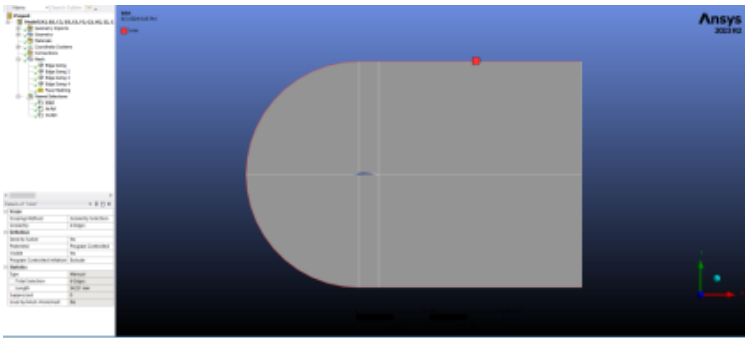

Figure II.24: Inlet named selection

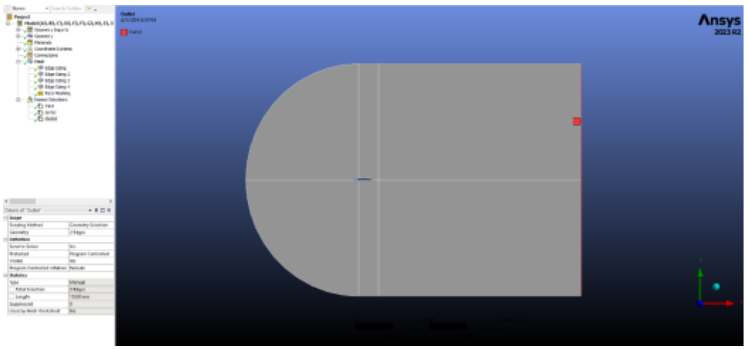

Figure II.25: Outlet named selection

But the airfoil changes for each configuration in this one the selection is simple:

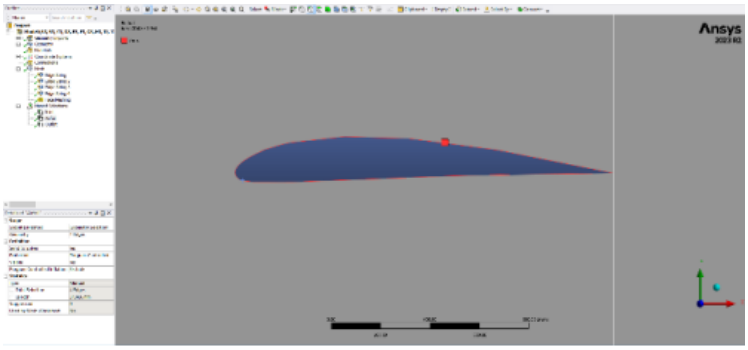

Figure II.26: Airfoil named selection

We also use the face meshing option with a quadrilateral method to have a structured mesh that use quad elements.

7.2 One and two SLATs configuration meshing:

Just like in the geometry creation this 2 follow the same method we will only be explaining the 2 SLATs steps.

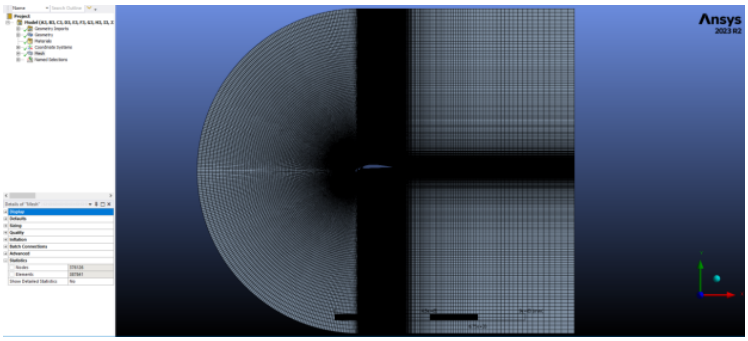

Figure II.27: Two slots full mesh

Since the airfoil and slats are uncastrated in a zone of their own, we can't use the bias factor to create our inflation layer and thus we must use the inflation option for each part all of them. We only use the face meshing on the outer region because of the complexity of the intern region the meshed didn't not succeed in structuring it wish leave us with a semi structured mesh that is because we need to use smaller element size in that region wish we are not able, the minimum we can use is a 1mm.

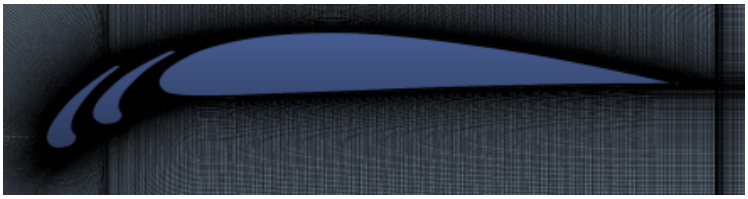

Figure II.28: zoom one the airfoil mesh for 2 SLATs

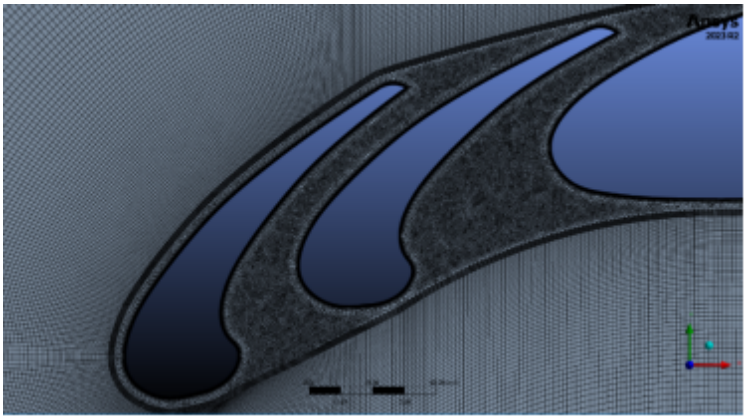

Figure II.29: zoom in the 2 SLATs

The same for the 1 slot configuration:

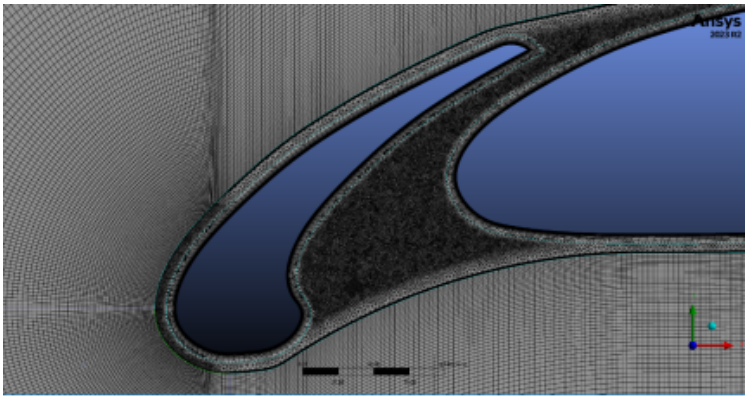

Figure II.30: zoom in the 1 SLATS

7.3 Closed SLATs configuration meshing:

This configuration also has a zone around the airfoil so we will have to use the inflation tool, the reason why is because the of dip at the tip of the SLATs that dip need a great deal of elements to be properly modelized.

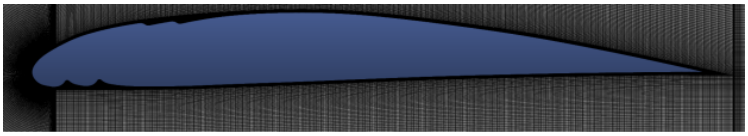

Figure II.31: Closed SLATs airfoil Mesh

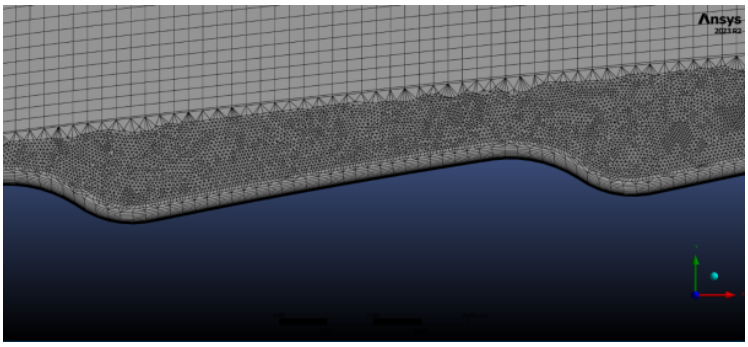

Figure II.32: Closed SLATs top side zoom

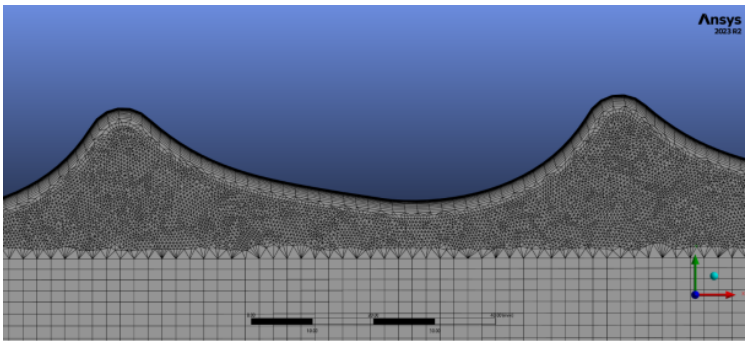

Figure II.33: Closed SLATs Bot side zoom

7.4 Inflation Parameters:

All inflation has the same parameter:

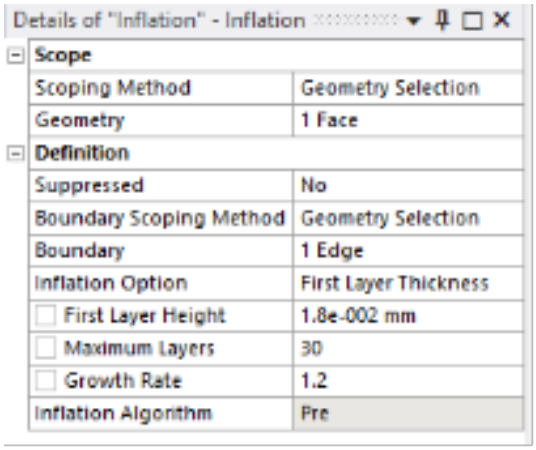

Figure II.34: Inflation Details.

8 Navier-Stokes Equations:

8.1 Conservation of Mass (Continuity Equation)

The principle of conservation of mass states that mass cannot be created or destroyed in a closed system. For a fluid, this principle is expressed mathematically by the continuity equation. For an incompressible fluid, where the density (ρ) is constant, the continuity equation simplifies to:

$$\nabla \cdot \mathbf{u} = 0 \tag{II.3}$$

where:

- $\nabla \cdot \mathbf{u}$: Divergence of the velocity field
- $\mathbf{u}$: Velocity vector

Here, u = (u, v, w) is the velocity vector with components in the x, y, and z directions, respectively. This equation indicates that the divergence of the velocity field is zero, meaning that the fluid's volume remains constant over time.

For compressible flows, where the density (ρ) can vary with time and space, the continuity equation is :

$$\frac{\partial \rho}{\partial t} + \nabla \cdot (\rho \mathbf{u}) = 0 \tag{II.4}$$

where:

- $\frac{\partial \rho}{\partial t}$: Time rate of change of density
- $\nabla \cdot (\rho \mathbf{u})$: Divergence of the mass flux
- ρ: Density of the fluid
- $\mathbf{u}$: Velocity vector

This form accounts for changes in density and ensures that the mass of the fluid is conserved as it flows through different regions.

8.2 Conservation of Momentum (Navier-Stokes Equations):

The conservation of momentum is derived from Newton's second law of motion, which states that the rate of change of momentum of a fluid element is equal to the sum of the forces acting on it. The Navier-Stokes equations describe this principle for fluid motion :

$$\frac{\partial(\rho \mathbf{u})}{\partial t} + \nabla \cdot (\rho \mathbf{u}\mathbf{u}) = -\nabla p + \nabla \cdot \tau + \mathbf{f} \tag{II.5}$$

where:

- $\frac{\partial(\rho \mathbf{u})}{\partial t}$: Time rate of change of momentum
- $\nabla \cdot (\rho \mathbf{u}\mathbf{u})$: Divergence of the momentum flux
- $-\nabla p$: Gradient of pressure
- $\nabla \cdot \tau$: Divergence of the stress tensor
- $\mathbf{f}$: Body forces (e.g., gravity)

For a Newtonian fluid, where the stress tensor (τ) is linearly related to the strain rate, the components of the Navier-Stokes equations in Cartesian coordinates are:

$$\rho \left(\frac{\partial u}{\partial t} + u\frac{\partial u}{\partial x} + v\frac{\partial u}{\partial y} + w\frac{\partial u}{\partial z} \right) = -\frac{\partial p}{\partial x} + \mu \left(\frac{\partial^2 u}{\partial x^2} + \frac{\partial^2 u}{\partial y^2} + \frac{\partial^2 u}{\partial z^2} \right) + f_x \tag{II.6}$$

$$\rho\left(\frac{\partial v}{\partial t}+u\frac{\partial v}{\partial x}+v\frac{\partial v}{\partial y}+w\frac{\partial v}{\partial z}\right)=-\frac{\partial p}{\partial y}+\mu\left(\frac{\partial^2 v}{\partial x^2}+\frac{\partial^2 v}{\partial y^2}+\frac{\partial^2 v}{\partial z^2}\right)+f_y \tag{II.7}$$

$$\rho\left(\frac{\partial w}{\partial t}+u\frac{\partial w}{\partial x}+v\frac{\partial w}{\partial y}+w\frac{\partial w}{\partial z}\right)=-\frac{\partial p}{\partial z}+\mu\left(\frac{\partial^2 w}{\partial x^2}+\frac{\partial^2 w}{\partial y^2}+\frac{\partial^2 w}{\partial z^2}\right)+f_z \tag{II.8}$$

where:

- ρ: Density of the fluid
- u, v, w: Velocity components in the x, y, z directions, respectively
- $\frac{\partial u}{\partial t}, \frac{\partial v}{\partial t}, \frac{\partial w}{\partial t}$: Time rate of change of velocities u, v, w
- $u\frac{\partial u}{\partial x}, v\frac{\partial u}{\partial y}, w\frac{\partial u}{\partial z}$: Advective terms of velocity u
- $u\frac{\partial v}{\partial x}, v\frac{\partial v}{\partial y}, w\frac{\partial v}{\partial z}$: Advective terms of velocity v
- $u\frac{\partial w}{\partial x}, v\frac{\partial w}{\partial y}, w\frac{\partial w}{\partial z}$: Advective terms of velocity w
- $-\frac{\partial p}{\partial x}, -\frac{\partial p}{\partial y}, -\frac{\partial p}{\partial z}$: Pressure gradients in the x, y, z directions
- μ: Dynamic viscosity of the fluid
- $\frac{\partial^2 u}{\partial x^2}, \frac{\partial^2 u}{\partial y^2}, \frac{\partial^2 u}{\partial z^2}$: Laplacian terms (viscous diffusion terms) of velocity u
- $\frac{\partial^2 v}{\partial x^2}, \frac{\partial^2 v}{\partial y^2}, \frac{\partial^2 v}{\partial z^2}$: Laplacian terms (viscous diffusion terms) of velocity v
- $\frac{\partial^2 w}{\partial x^2}, \frac{\partial^2 w}{\partial y^2}, \frac{\partial^2 w}{\partial z^2}$: Laplacian terms (viscous diffusion terms) of velocity w
- f_x, f_y, f_z: Body force components (e.g., gravity) acting in the x, y, z directions

8.3 Conservation of Energy:

The conservation of energy principle states that the total energy of an isolated system remains constant. For fluid flow, this principle is expressed through the energy equation, which accounts for the conservation of thermal energy, kinetic energy, and potential energy. The

general form of the energy equation for a compressible fluid is:

$$\frac{\partial(\rho E)}{\partial t} + \nabla \cdot (u(\rho E + p)) = \nabla \cdot (k \nabla T) + \Phi + u \cdot \mathbf{f} \qquad \text{(II.9)}$$

where:

- $\frac{\partial(\rho E)}{\partial t}$: Time rate of change of total energy density
- ρ: Density of the fluid
- E: Total energy per unit mass (including internal energy and kinetic energy)
- u: Velocity vector of the fluid
- p: Pressure
- k: Thermal conductivity
- T: Temperature
- Φ: External heat sources (e.g., heat generation)
- $\mathbf{f}$: Body force vector (e.g., gravity)

9 Solver Configuration: [6]

After creating a mesh that is both structured and with a inflation layer that properly solve our boundary layer it time import our mesh into the FLUENT solver and prepare our setup, us we said the meshing processes is the hardest and most time consuming one after that come the setup where each option can dramatically alter our result from choosing between a pressure based solver or a density based one to the type of turbulence model, in this chapter we look at the most important option given the different type and explaining why we chose that option:

9.1 Type of solver:

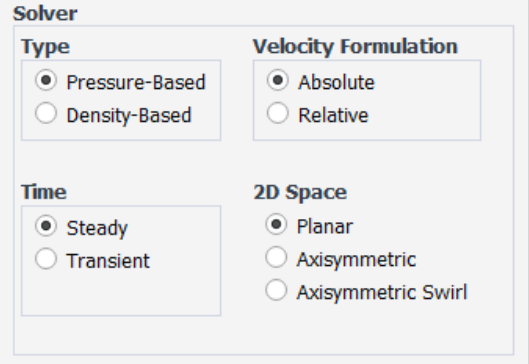

Figure II.35: Fluent solver panel

We have 2 types of solvers; one that a is a pressure-based solver and the other a density one.

9.1.1 Pressure-based solver:

The pressure-based enables the pressure-based Navier-Stokes solution algorithm, this solver is typically used for incompressible flows or flows with low Mach numbers (V<100m/s) It does that by solving the momentum equations and the pressure-based continuity equation. **Advantages of pressure-based solver:** This solver is highly efficient and accurate for incompressible and low-speed compressible flows, also the pressure-based solver is generally more stable for a wide range of flow problems, including laminar and turbulent flows, finally It is robust and can handle complex geometries and boundary conditions effectively.

9.1.2 Density-based solver:

Enables the density-based Navier-Stokes coupled solution algorithm, and is primarily used for compressible flows, where the Mach number is high (V>100m/s), this solver solves the governing equations for mass, momentum, and energy using a density-based formulation. It directly solves the conservation equations for density, momentum, and energy, and uses algorithms designed to capture shocks wave and

discontinuities. **Advantages of density-based solver:** This solver is used for high-speed compressible flow such as those encountered in aerospace application because it can capture the shock wave produced by supersonic and transonic flows, but also is more suitable for modeling combustion.

9.2 Choosing Between the two solvers:

The pressure base solver is the clear better choice for our application not only we are a low Mach number because our free stream velocity is only 10m/s that mean we are in the incompressible flow we also don't do any heat transfer.

9.3 Velocity formulation:

This one is clear and cut one option enables the use of the absolute velocity formulation the other enables the use of the relative velocity formulation, our is a Absolut velocity formulation.

9.4 Time options:

contains options related to time dependence, we have the steady state where the solver assumes that the flow conditions do not change with time. It solves the governing equations of fluid flow with the assumption that the flow has reached an equilibrium, while the Transient one accounts for time-dependent changes in the flow field and capture the evolution of the flow variables as they change over time. We used the steady stat solver because an airfoil analysis isn't time dependent when using a rans model and the simulations are generally faster and require less computational resources compared to transient simulations.

9.5 Turbulence model:

For our Viscous model we have chosen the SST $k-\omega$ and hirs why: From the get go we can eliminate all URANS model and that includes DES and LEA because all of them require a 3D mesh that is because EDDYs are a

3D Fennomen, so the minimums element count that new need is at least 3million element and that is considered a coarse mesh in LES simulation, so that leave us with the RANS models, to choose between them we need to remember 2 points of order that Comme simulating and airfoil. We need a model that is Robust and Stabile because we are dealing with experimental designee without access to real world data. We need the model to be sensitive to adverse pressure gradients. The models that most answer those requirements is the SST $k-\omega$ model because of the flow separation that occur at the high angle of attack that we will need good adverse flow direction behind the airfoil. But why not another type of $k-\omega$ model simply the SST was developed for our precise application and is an industry standard, there is also the GEKO type but this one needs to be tailored and that need experimental data that we don't have access to. We introduce no change to the default model because us we said it is already been modified to reflect industry standard by the Ansys team that collect information from different company.

Figure II.36: Fluent Viscous model's panel

9.6 Boundary condition:

Our boundary's condition is already assigned from the named selection that we created in the Meshing phase we only need to check that they are properly assigned wish they are:

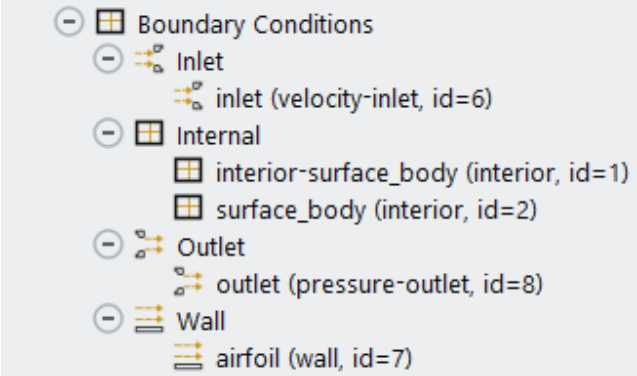

Figure II.37: Fluent Dropdown boundary's conditions.

From the inlet boundary condition we can control the free stream velocity, in there we use a magnitude and direction specification method that so we can change the Angle of attack by changing the direction of the air, for the velocity magnitude it is different for each configuration the reason is because of the varying chord length we change the velocity to keep the Reynold numbers the same (106

) but the all go from 9,5 m/s to 10 m/s wish is a small difference, to change the angle just calculate his X-component and Y component and right them in the correct case. Fluent Velocity inlet Panel

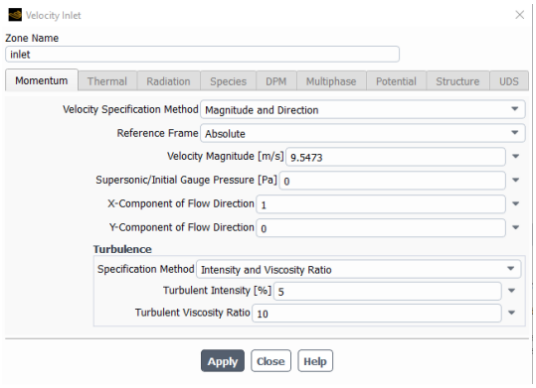

Figure II.38: Fluent Velocity inlet Panel

9.7 Reference value option:

The Reference Values task page allows you to set the reference quantities used for computing normalized flow field variables, in this page we us the inlet boundary condition us Reference Area this will be sued to calculate the values but the reference length and area will not be set by computing the reference values from a boundary condition ; we must set these manually, so the are is the chord length of our airfoil and the length stay the same.

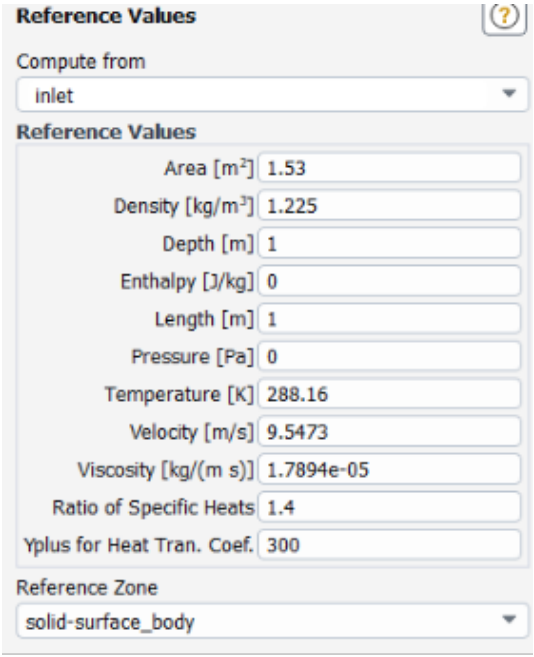

Figure II.39: Fluent Reference values

9.8 Materials selection:

This where we create and configures our materials properties you can add both solid and fluid materials, for our case we only need to create a fluid that is the air that will fill our internal boundary condition, this air will be at a temperature of 10°c, wish is the default one in the solver.

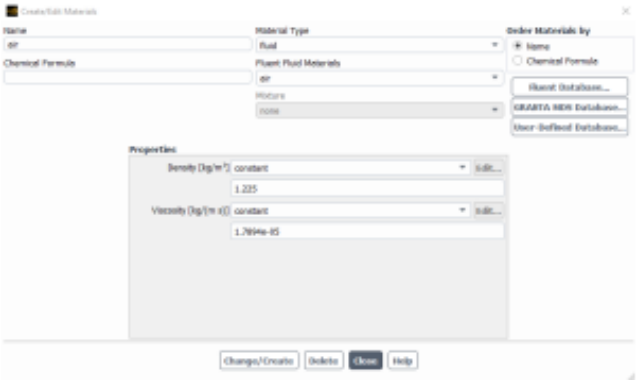

Figure II.40: Fluent materials creation and editing panel

10 Solution methods: [6]

the Solution Methods task page allows you to specify various parameters associated with the solution method to be used in the calculation since we use a pressure-based solver, we the solution methods is already set for the best method that align with our solver type but we can still make change, notably we have 3 option that greatly alter the result of our simulation this are the scheme and pseudo time method and also the discretization schemes:

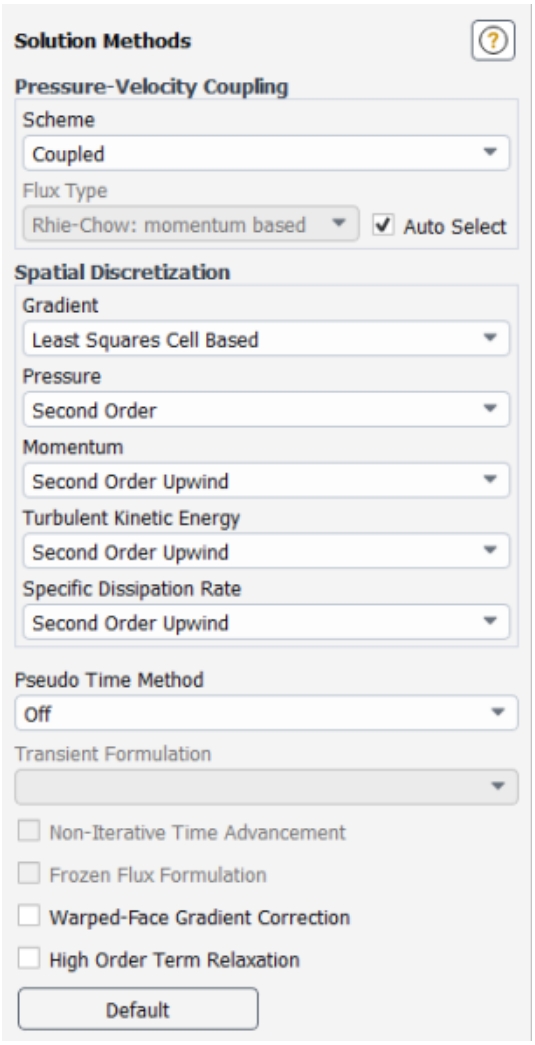

Figure II.41: Fluent Solution methods panel

10.1 Schemes type:

For the scheme we have 4 choices:

10.1.1 SIMPLE and SIMPLEC scheme:

Thos 2 are a solver that work iteratively by separately updating the pressure and velocity fields to ensure mass conservation and stable solutions, while the SIMPLC is a variant that modifies the correction steps to accelerate convergence.

10.1.2 Coupled scheme:

The coupled algorithm solves the momentum and pressure-based continuity equations together, enhancing convergence speed and stability.

10.1.3 PISO (Pressure-Implicit with Splitting of Operators):

This scheme method is a modified SIMPLE scheme that is used for transient flow wish our simulation is not.

10.1.4 Choosing our scheme:

For our simulation we decided to use the coupled scheme over the SIMPLE and SIMPLEC, the first reason is because the coupled one give better result for higher computational cost, a cost that we can afford. In the momentum equations:

$$aPu = \sum_{n_b} a_{n_b} u_{n_b} + \sum_{p_f} f_{p_f} A \cdot i + S \tag{II.10}$$

where:

- aPu: Total force applied to the system
- n_b: Index for boundary nodes
- a_{n_b}: Coefficient associated with boundary nodes
- u_{n_b}: Displacement of boundary nodes

- p_f: Index for applied forces
- f_{p_f}: Applied force magnitude
- A: Area
- i: Direction vector
- S: Any additional source term

the pressure gradient for component k is of the form:

$$\sum_{p_f} f_{p_f} A_k^f = -\sum_a u_k p_p j \tag{II.11}$$

Where $a_{u_k p}$ is the coefficient derived from the Gauss divergence theorem and coefficients of the pressure interpolation schemes. Finally, for any ith cell, the discretized form of the momentum equation for component U_k is defined as:

$$P_f = \frac{P_{c0} \div a_{p,c0} + P_{c1} \div a_{p,c1}}{\frac{1}{a_{p,c0}} + \frac{1}{a_{p,c1}}} \tag{II.12}$$

where:

$$\begin{aligned} P_f &: \text{Resultant value} \\ P_{c0}, P_{c1} &: \text{Values from sources } c0 \text{ and } c1, \text{ respectively} \\ a_{p,c0}, a_{p,c1} &: \text{Coefficients associated with sources } c0 \text{ and } c1 \end{aligned}$$

$$\sum_{i,j} a_{ij} u_k u_{kj} + \sum_{i,j} a_{ij} u_k p_j = b_i u_k \tag{II.13}$$

In the continuity equation:

$$\sum_{f=1}^{\text{Nfaces}} J_f A_f = 0 \tag{II.14}$$

The balance of fluxes is replaced using the flux expression:

$$J_f = \frac{\rho_f (a_{p,c0} \mathbf{v}_{n,c0} + a_{p,c1} \mathbf{v}_{n,c1})}{a_{p,c0} + a_{p,c1}} + d_f \left((p_{c0} + (\nabla p)_{c0} \cdot \vec{r}_0) - (p_{c1} + (\nabla p)_{c1} \cdot \vec{r}_1) \right)$$

$$= \mathrm{J}_f + d_f (p_{c0} - p_{c1}) \tag{II.15}$$

Resulting in the discredited form

$$\sum_{k}\sum_{j} a_{ij}^{p_{uk}} u_{kj} + \sum_{j} a_{ij}^{p_p} p_j = b_i^p \tag{II.16}$$

As a result, the overall system of equations, after being transformed to the -form, is presented as:

$$\sum_{j} [A]_{ij} \vec{X}_j = \vec{B}_i \tag{II.17}$$

Where the influence of a cell i on a cell j has the form

$$[A] = \begin{bmatrix} a_{ij}^{pp} & a_{ij}^{pp} & a_{ij}^{pv} & a_{ij}^{pw} \\ a_{ij}^{up} & a_{ij}^{uw} & a_{ij}^{\psi v} & a_{ij}^{uw} \\ a_{ij}^{vp} & a_{ij}^{wu} & a_{ij}^{vv} & a_{ij}^{vw} \\ a_{ij}^{wp} & a_{ij}^{w} & a_{ij}^{wv} & a_{ij}^{ww} \end{bmatrix}$$

And the unknown and residual vectors have the form:

$$\vec{X}_j = \begin{pmatrix} p_i' \\ u_i' \\ v_i' \\ w_i' \end{pmatrix} \tag{II.18}$$

$$\vec{B}_i = \begin{pmatrix} -r_i^p \\ -r_i^u \\ -r_i^v \\ -r_i^w \end{pmatrix} \tag{II.19}$$

10.2 Pseudo time method:

We will not be using this method because it basically Instead of directly solving the steady-state equations, the pseudo-time method solves a modified set of transient equations with an artificial time-stepping process until a steady state is reached this cause divergence and has a higher computational cost with adding mush precision to our result because an airfoil simulation, we said is not time dependent.

10.3 Discretization schemes:

We will be using Second-Order Upwind Scheme for the discretization because it is the best compromise between the 4 different schemes wish all work by estimating the value at the cell face of neighboring cells some more then other, our scheme uses a linear interpolation between cell centers wish give us Higher Accuracy for not too much Computational Cost.

11 Solution initialization: [6]

The initialization is the setting initial values for various flow variables (velocity, pressure, temperature...) for the domain. These initial values serve as the starting point for the iterative solver, in this we have 2 methods; that is the standard one wish consist of manually setting the values, and the second one wish is the hybrid method, this method automatically create an initial solution using a robust algorithm based one LaPlace equation to generate a starting field this method is the most used for general application and will be the one we will use.

12 Residuals monitoring: [6]

In a CFD analysis, the residual measures the imbalance of a variable in each cell, every cell in your model will have its own residual value for each of the equations being solved. a typical CFD simulation includes equations for momentum, pressure, and turbulence, and the solver performs iterative solutions of these equations, the residuals plot shows the difference between successive solutions of these equations. In an iterative numerical solution, the residual will never be exactly zero, However the lower the residual value is the more accurate is the solution. For our Convergence criteria we will us the continuity residuals which represents the conservation of mass between and it is done by monitoring the imbalance of mass fluxes entering and leaving each cell within the domain. The reason why we use this criterion alone is because it is

the hardest one to converge meaning that when attaining these criteria, we converged the other already converged, ANSYS use a default value of 1E-6, we will consider those value as coarse criteria. We used a different criterion for each configuration, for our 2 SLAT and 1 SLAT configuration we use a 1E-8 compared to the default value this one is rather fin, for the No SLAT configuration and the closed SLATs one we use a 1E-7 and 1E-6 respectively because the last configuration is just to show the default of our design.

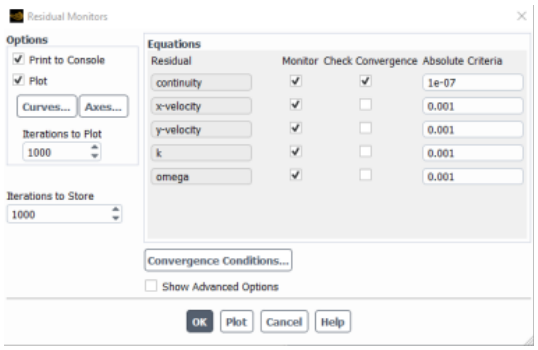

Figure II.42: Fluent Residual monitors plan.

13 Running the Calculation:

This task page allows you to start the solver iterations, in a steady flow calculation it contains settings for running, reporting, and updating the calculation, this setting are: Number of Iterations; sets the number of iterations to be performed, Reporting Interval; sets the number of iterations that will pass before convergence monitors will be printed and plotted, Profile Update Interval; This interval also controls the frequency at which Named Expression values are updated.

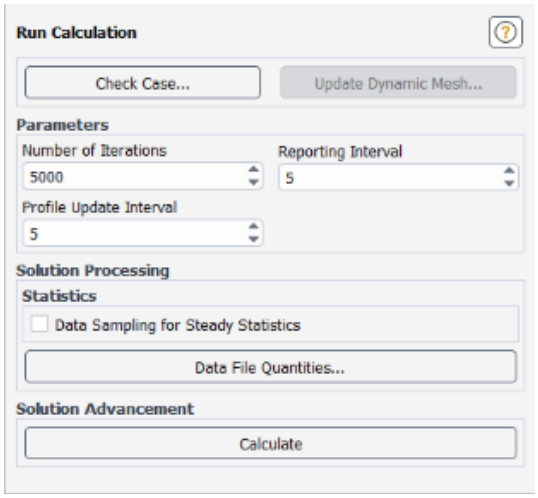

Figure II.43: Fluent Calculation Startup panel

We set our number of iterations to 15000 iterations to make sur all configuration has converged with a 5-iteration delay between report us to not clutter our fill with futile details. From her our Fluent is setup we go to Ansys workbench and press the update button and let them calculate.

14 Conclusion

We detailed the setup process for our Fluent simulation, highlighting the critical choices made at each stage. We began with the geometry and meshing, ensuring a detailed and accurate representation of the physical domain. The importance of these initial steps cannot be overstated, as even small complexities in the geometry, such as those observed in the closed SLATs configuration, can significantly impact the computational cost and calculation time. Additionally, we configured essential physical models and boundary conditions tailored to our specific study requirements. Solver settings were optimized for stability and convergence, and we utilized Fluent's post-processing tools for effective visualization and analysis. This comprehensive setup establishes a robust foundation for our research and ensures reliable outcomes,

underscoring the time-intensive nature of generating a good pool of data.

Chapter III

Result exposition and discussion

1 USA-35B Simulation results:

With the UIUC Airfoil Data Site we have a base line to compare our CFD result too so we will put them side by side and go on to explain the similarity and difference that arise from using different method of calculation. To note we will be addressing our result, our result will be result 1 and the data base result will be result 2.

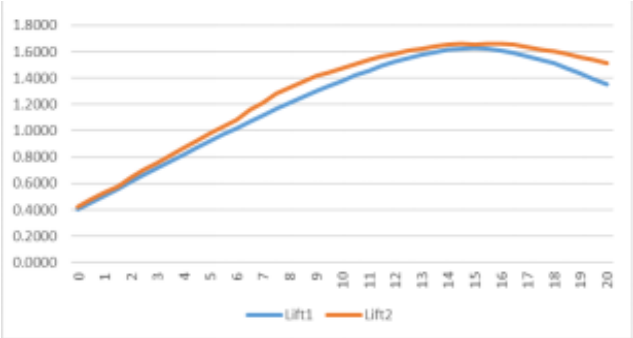

Figure III.1: Chart for the Lift coefficient for AOA.

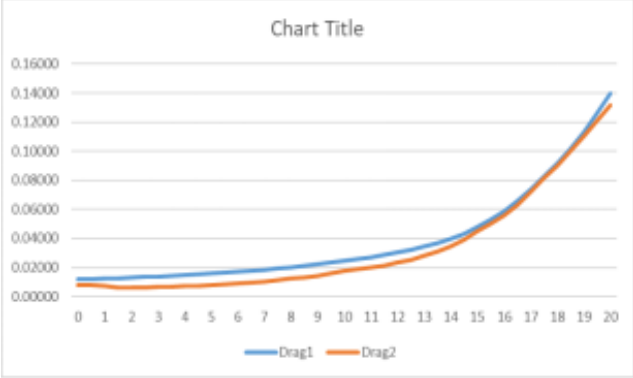

Figure III.2: Chart for the Drag coefficient for AOA.

Us expected the Drag result all mush higher for the CFD result, for us we explained before XFoil cannot resolve the wake turbulence effect so it underpredict the Drag coefficient and overpredicts the maximum lift coefficient, the difference is between 5lift coefficient wish is acceptable range, even though there are no strict criteria some paper accept result up to 20The data is clearer to see with a chart, by looking at it we

Table III.1: USA-35B Simulation results for each AOA.

Angle	CL1	CL2	CD1	CD2	CL1/CD1	CL2/CD2	DELTA
0	0.4003	0.4217	0.01192	0.00801	33.58637	52.64669	19.06032
0.5	0.4537	0.4786	0.01213	0.00768	37.39075	62.31771	24.92696
1	0.5070	0.5340	0.01239	0.00702	40.92261	76.06838	35.14577
1.5	0.5600	0.5797	0.01268	0.00606	44.15913	95.66007	51.50094
2	0.6128	0.6475	0.01302	0.00618	47.08384	104.77346	57.68962
2.5	0.6654	0.7031	0.01339	0.00636	49.70125	110.55031	60.84906
3	0.7176	0.7590	0.01380	0.00655	52.01018	115.87786	63.86768
3.5	0.7695	0.8148	0.01425	0.00676	54.01441	120.53254	66.51813
4	0.8210	0.8700	0.01473	0.00703	55.71814	123.75533	68.03719
4.5	0.8719	0.9245	0.01526	0.00737	57.13297	125.44098	68.30801
5	0.9225	0.9781	0.01583	0.00779	58.26168	125.55841	67.29673
5.5	0.9725	1.0306	0.01645	0.00830	59.12808	124.16867	65.04060
6	1.0217	1.0831	0.01710	0.00880	59.73952	123.07955	63.34003
6.5	1.0703	1.1609	0.01781	0.00958	60.10842	121.17954	61.07112
7	1.1181	1.2111	0.01856	0.01023	60.24489	118.38710	58.14221
7.5	1.1649	1.2815	0.01936	0.01154	60.16703	111.04853	50.88150
8	1.2108	1.3284	0.02023	0.01234	59.86589	107.64992	47.78403
8.5	1.2556	1.3744	0.02115	0.01315	59.36259	104.51711	45.15452
9	1.2990	1.4185	0.02214	0.01403	58.65991	101.10478	42.44486
9.5	1.3411	1.4452	0.02322	0.01608	57.75491	89.87562	32.12071
10	1.3815	1.4777	0.02438	0.01747	56.66356	84.58500	27.92145
10.5	1.4201	1.5088	0.02565	0.01857	55.37454	81.24933	25.87478
11	1.4568	1.5363	0.02703	0.01994	53.88604	77.04614	23.16010
11.5	1.4911	1.5633	0.02857	0.02141	52.19431	73.01728	20.82297
12	1.5227	1.5842	0.03028	0.02342	50.29343	67.64304	17.34961
12.5	1.5516	1.6086	0.03221	0.02535	48.17465	63.45562	15.28097
13	1.5766	1.6251	0.03440	0.02805	45.83752	57.93583	12.09831
13.5	1.5978	1.6387	0.03692	0.03123	43.27217	52.47198	9.19981
14	1.6142	1.6544	0.03988	0.03449	40.47341	47.96753	7.49412
14.5	1.6249	1.6619	0.04340	0.03880	37.44165	42.83247	5.39082
15	1.6284	1.6570	0.04763	0.04478	34.18727	37.00313	2.81585
15.5	1.6239	1.6624	0.05276	0.04992	30.77608	33.30128	2.52520
16	1.6110	1.6620	0.05889	0.05591	27.35620	29.72635	2.37015
16.5	1.5914	1.6546	0.06594	0.06299	24.13458	26.26766	2.13308
17	1.5674	1.6325	0.07373	0.07227	21.25794	22.58890	1.33096
17.5	1.5403	1.6145	0.08220	0.08131	18.73863	19.85611	1.11748
18	1.5102	1.5997	0.09142	0.09022	16.51969	17.73110	1.21141
18.5	1.4761	1.5809	0.10161	0.09992	14.52704	15.82166	1.29462
19	1.4372	1.5605	0.11307	0.11016	12.71089	14.16576	1.45487
19.5	1.3943	1.5391	0.12585	0.12073	11.07891	12.74828	1.66937
20	1.3510	1.5159	0.13958	0.13186	9.67918	11.49628	1.81710

discern that they follow the same trajectory and that in itself a good sign of accuracy. Max lift or drag alone don't tell us anything about the effectiveness of an airfoil, for that we need the Lift/Drag Coefficient for the angle:

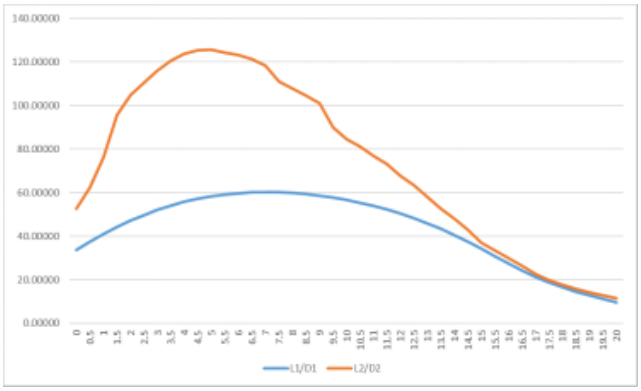

Figure III.3: Chart for the Lift to Drag Coefficient for AOA.

When the Lift to Drag ratio is put on juxtaposition to each other the full effect of Drag underprediction become clear, where the max LIFT to DRAG for the Database result is 120 at 5° our CFD result show the max LIFT/DRAG coefficient is 60 at 7°, to mean 2 time the value and 2° degrees after. We can deduce 2 general point to integrate in our future result interpretation:

- although not totally accurate XFoil result and the university of Illinoi Database, they are accurate enough for the first step of airfoil selection and study especially at low Angle of attack.
- Applying a 15with a Lift to Drag Ratio. To finish we give a graphical representation of velocity distribution:

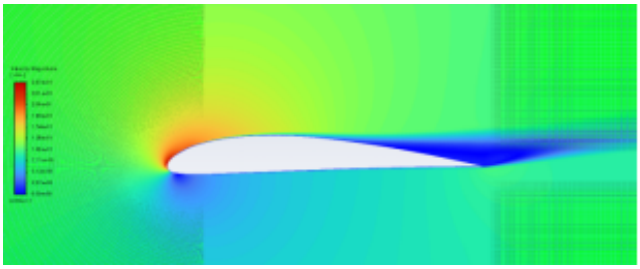

Figure III.7: The contour plots of velocity distribution at 15°

Figure III.4: The contour plots of velocity distribution at 0°

Figure III.5: The contour plots of velocity distribution at 5°

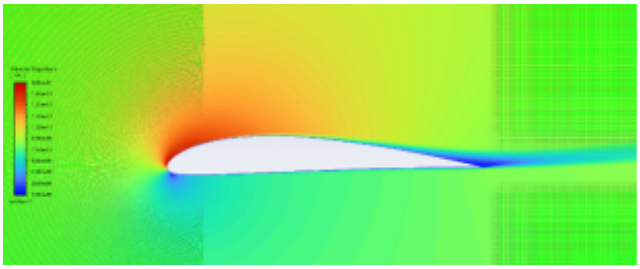

Figure III.6: The contour plots of velocity distribution at 10°

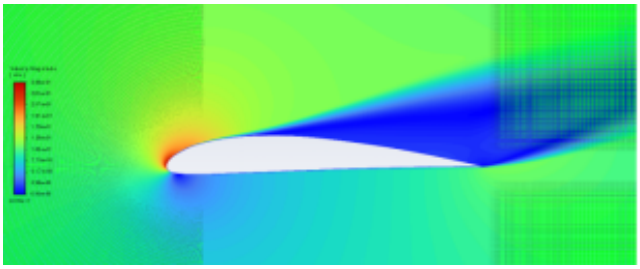

Figure III.8: The contour plots of velocity distribution at 20°

2 V-2Closed SLAT Configuration Results:

All results are presented in this Table, for each angle of attack with have the Drag and Lift coefficient, and the Lift to drag ratio with the number of iterations need to get there. The first thing that jump to us

Table III.2: Closed SLATs Simulation results for each AOA.

Angle	CL	CD	CL/CD	Residuals	Iterations
0	0.36323942	0.013616328	26.67675309	4.79E-05	15000
2.25	0.62349895	0.015021131	41.50812279	1.47E-05	15000
5	0.8762636	0.017771703	49.3066759	7.32E-06	15000
7.5	1.1136567	0.021959871	50.71326239	1.28E-06	15000
10	1.3233561	0.027945349	47.35514665	1.95E-07	15000
12.5	1.4867824	0.036977869	40.20735754	1.03E-06	15000
15	1.571331	0.05275741	29.78408152	9.82E-08	1735
17.5	1.5652966	0.079972637	19.57290217	2.60E-07	15000
20	1.0093495	0.21514417	4.691502912	4.59E-04	15000

looking at our table is the residuals, we explained in the setup of fluent that a Continuity residual of 1E-05 is an industry standard for our other Configuration we went for stricter Criteria that are not needed for these analyses since its pint is to show us our designee mistake and to clarify the negative effect the admission of the Slot is for the original airfoil.

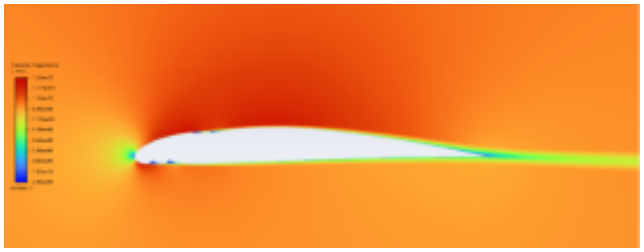

Figure III.9: The contour plots of velocity distribution at 0° in closed SLAT.

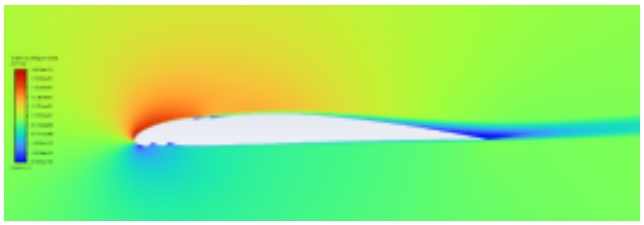

Figure III.10: The contour plots of velocity distribution at 10° in closed SLAT.

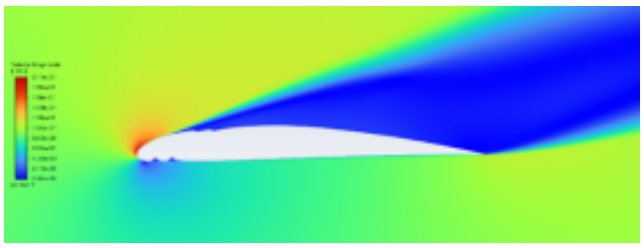

Figure III.11: The contour plots of velocity distribution at 20° in closed SLAT.

3 Comparison between Closed 2 SLAT and No SLAT Configuration:

In this Table we put the result for the Closed Slot Configuration and the no Slot configuration to draw a better picture of the losses of performance: Closed SLOTs are configuration 1 and No slot is configuration 2.

Table III.3: result comparison for USA-35B and Closed SLATs.

Angle	CL1	CD1	CL2	CD2	CL1/CD1	CL2/CD2
0	0.36323942	0.013616328	0.400313309	0.01191892	26.67675309	33.58637387
2.25	0.62349895	0.015021131	0.665359159	0.013387171	41.50812279	49.70125024
5	0.8762636	0.017771703	0.922507544	0.015833864	49.3066759	58.26168022
7.5	1.1136567	0.021959871	1.164877936	0.019360736	50.71326239	60.16702669
10	1.3233561	0.027945349	1.381474008	0.024380291	47.35514665	56.66355668
12.5	1.4867824	0.036977869	1.551586674	0.032207531	40.20735754	48.17465381
15	1.571331	0.05275741	1.628442008	0.047632991	29.78408152	34.18727143
17.5	1.5652966	0.079972637	1.540306894	0.082199545	19.57290217	18.73863032
20	1.0093495	0.21514417	1.350986064	0.139576441	4.691502912	9.679184075

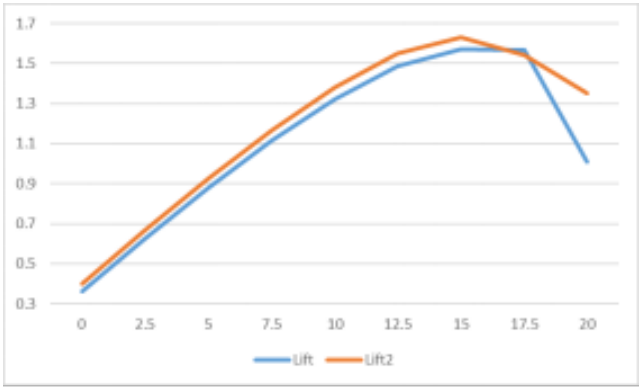

Figure III.12: Chart for the Lift coefficient for AOA in SLATs and no SLAT configuration.

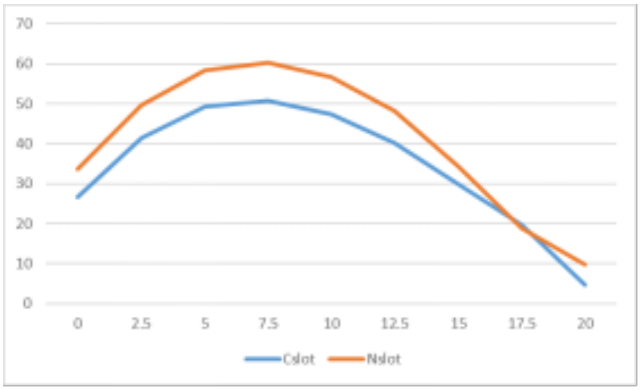

Figure III.13: CChart for the Lift to Drag Coefficient for AOA in SLATs and no SLAT configuration.

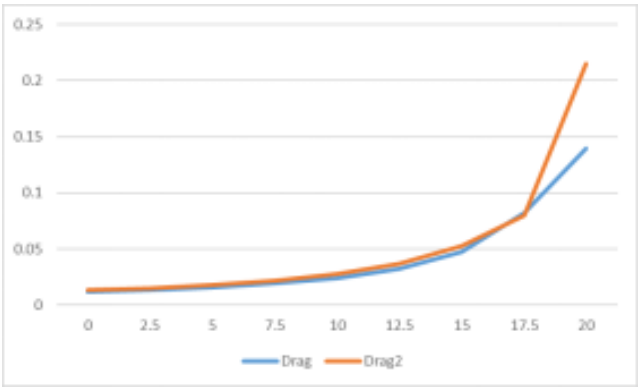

Figure III.14: Chart for the Drag coefficient for AOA in SLATs and no SLATS configuration

Once again, we can can't get mush from comparing the Drags and the lifts coefficient for only the Lift to drag coefficient can tell us the effectiveness of an airfoil. What we can get from the Lift coefficient comparisons is that the Closed Slat configuration has a lower Lift Coefficient with a much higher Drag, at average of 12decrease of lift coefficient and a 13% increase of Drag coefficient. When zooming in the Velocity magnitude Contour distribution we can see how the form of the SLOTs causes pocket of back flow that induce a Flow separation mush sooner than that it should.

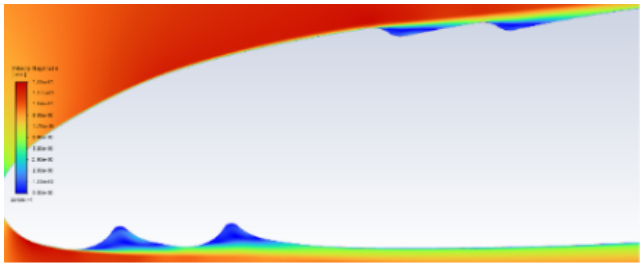

Figure III.15: The contour plots of velocity distribution in the Closed SLATs region.

4 Two SLATs Configuration Results:

All results are presented in this Table, for each angle of attack with have the Drag and Lift coefficient with the number of iterations need to get there.

Table III.4: Two SLATs Simulation Lift to Drag for each AOA.

Alpha, L/D 1 SLOT, Iteration			Alpha, L/D 1 SLOT, Iteration		
Alpha	L/D 1 SLOT	Iteration	Alpha	L/D 1 SLOT	Iteration
20.00	32.42561054	810	25.25	26.98173694	1790
20.25	32.24266528	880	25.50	26.63979422	1570
20.50	32.05249808	870	25.75	26.24925237	1400
20.75	31.85468062	810	26.00	25.83440215	1350
21.00	31.65363336	990	26.25	25.34869551	1950
21.25	31.44822848	930	26.50	24.90521349	2000
21.50	31.23551897	970	26.75	24.45124366	2810
21.75	31.00860795	1080	27.00	23.91195456	2090
22.00	30.77727966	1100	27.25	23.53274359	2080
22.25	30.537057	1040	27.50	23.02965481	2300
22.50	30.29039856	1140	27.75	22.59806456	1600
22.75	30.03750543	1140	28.00	22.16939909	1590
23.00	29.77341652	1110	28.25	21.77887069	1740
23.25	29.50281646	1120	28.50	21.40454266	2290
23.50	29.2187493	1150	28.75	21.01196376	1810
23.75	28.92810406	1200	29.00	20.65538731	1940
24.00	28.62761566	1190	29.25	20.32161253	2010
24.25	28.33496977	1350	29.50	19.98783775	2230
24.50	28.02213532	1410	29.75	19.66339144	2280
24.75	27.69234375	1440	30.00	19.32770474	2370
25.00	27.35997908	1470			

All the simulation for this configuration successfully converged to a 1E-8 of continuity residuals, this mean is a testament to the clarity of our mesh specifically in the SLOT region for the was the most difficult to refine. We note that the average iteration number starts at around 1000 iteration in the lower angle of attack and grows with growing angle at around 2000 iteration needed to converge for the higher AOA. Showing the growing complexity of calculation caused by the steeper angle. Not mush can be said without comparing the configuration to another except that the airfoil without SLAT Max AOA is of 19 and thus entre STALL way before the 2 Slot configuration. When looking at the velocity and pressure distribution we can discern 2 zone of back flow in the SLOT Zone one is at the tip and of the SLAT and the other inside the internal curvature. This 2 Figure show us the zone that need to be ameliorated,

the inside curvature can't be flattened because of the need to retracted it but the tip can be changed by increasing the length of the SLAT and decreasing with it the width in the end, using sharp tip can also help, we used a rounded edge because of the difficulty of meshing sharp edges with inflation layer.

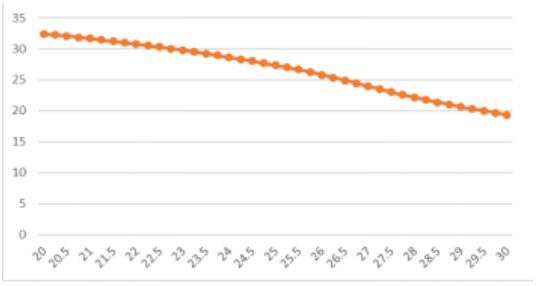

Figure III.16: Chart for the Lift to Drag coefficient for AOA in 2 SLATs.

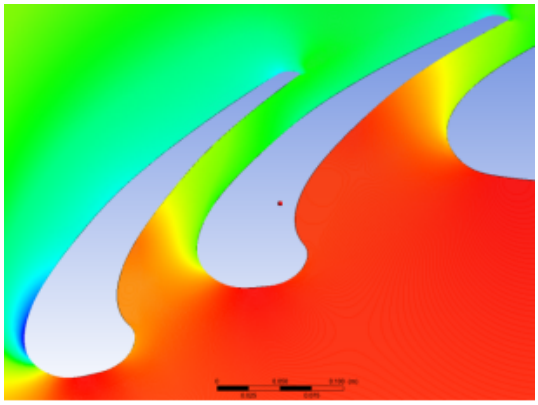

Figure III.17: The contour plots of pressure distribution in the Two SLATs region.

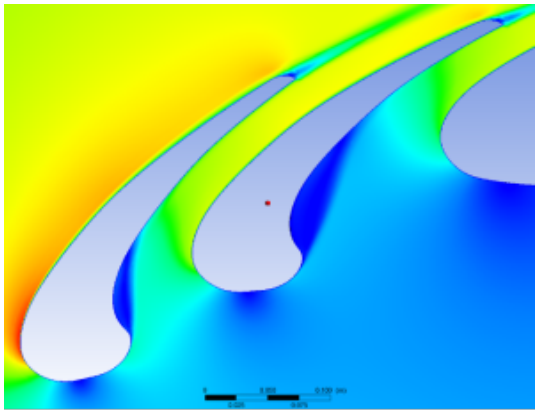

Figure III.18: The contour plots of pressure distribution in the Two SLATs region.

Note: Red is higher value while green and blue are lower. Finally we give the Lift and drag coefficient result for added details.

Table III.5: Two SLATs Simulation results for each AOA.

Alpha	CL	CD	Alpha	CL	CD
20.00	2.232574839	0.068852207	25.25	2.536103067	0.093993321
20.25	2.251677593	0.069835343	25.50	2.54517151	0.095540209
20.50	2.270468225	0.070835921	25.75	2.550204221	0.097153404
20.75	2.288695067	0.071847999	26.00	2.553896477	0.098856419
21.00	2.30674083	0.072874441	26.25	2.552094163	0.100679507
21.25	2.324492332	0.073914889	26.50	2.553403976	0.102524878
21.50	2.34183781	0.074973552	26.75	2.554325286	0.104466068
21.75	2.358685747	0.076065515	27.00	2.548640377	0.10658436
22.00	2.375127993	0.077171473	27.25	2.552449943	0.108463764
22.25	2.391151044	0.078303258	27.50	2.548001802	0.110640035
22.50	2.406737055	0.079455444	27.75	2.547370417	0.112725159
22.75	2.421721138	0.080623244	28.00	2.545517186	0.114821208
23.00	2.436139701	0.081822645	28.25	2.545300269	0.116870168
23.25	2.449993978	0.083042715	28.50	2.545520223	0.118924299
23.50	2.463216213	0.084302589	28.75	2.54494699	0.12111895
23.75	2.475810897	0.085584969	29.00	2.544575513	0.123191857
24.00	2.487542048	0.086893092	29.25	2.5453239	0.12531809
24.25	2.500235412	0.088238506	29.50	2.546516205	0.127403286
24.50	2.51110479	0.089611472	29.75	2.547200503	0.129540243
24.75	2.520944965	0.091034005	30.00	2.546810855	0.131769959
25.00	2.530021928	0.092471632			

5 1 SLOT Configuration Results:

All results are presented in this Table, for each angle of attack with have the Drag and Lift coefficient with the number of iterations need to get there.

Table III.6: One SLATs Simulation Lift to Drag for each AOA.

Alpha	L/D 1 SLOT	Iteration	Alpha	L/D 1 SLOT	Iteration2
20.00	31.10272113	1500	25.25	21.15713818	6795
20.25	30.64129397	1500	25.50	20.72859088	6810
20.50	30.16922831	1500	25.75	20.29349033	6750
20.75	29.695982	1535	26.00	19.89117559	6905
21.00	29.218429	1595	26.25	19.50114044	6950
21.25	28.73522564	1725	26.50	19.13439725	6915
21.50	28.2426344	6290	26.75	18.76760391	6930
21.75	27.75092092	6330	27.00	18.39744444	6985
22.00	27.25836967	6335	27.25	18.0282918	7095
22.25	26.76400706	6395	27.50	17.68303791	7230
22.50	26.22715437	1490	27.75	17.35672534	7155
22.75	25.74507643	1540	28.00	17.0458131	7340
23.00	25.26839145	1515	28.25	16.74396363	7190
23.25	24.79209487	1600	28.50	16.43774588	7210
23.50	24.29031963	1535	28.75	16.15217736	7375
23.75	23.86179089	1700	29.00	15.8676077	7375
24.00	23.39704493	1695	29.25	15.60317243	7340
24.25	22.93761196	1765	29.50	15.35471415	7460
24.50	22.47677958	1850	29.75	15.11402537	7500
24.75	22.03688488	6725	30.00	14.85717865	7595
25.00	21.5936396	6710			

Like we said in convergence criteria a residual of 1E-7 is a medium quality Criteria so don't be too disappointed that the result from 24.75° to 30° didn't converge all the way, but got stuck at continuity residuals of 5E-8, this failure to converge can have many reasons to it, the most common one is a too coarse of a mesh, Unfortunately we didn't have any more time to try to refine the mesh even more, and to note our criteria are too strict for most industry or even academic setting. Je like the 2 Slot configuration we can discern 2 zone of back flow in the SLOT, at the tip and inside the curvature here is visual representations of velocity

and pressure distribution, Red is higher value while green and blue are lower Value.

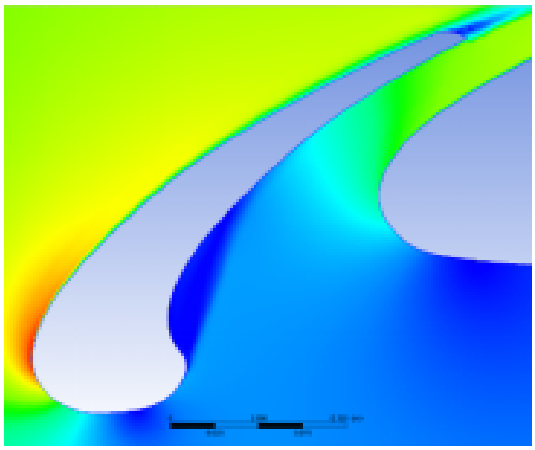

Figure III.19: The contour plots of velocity distribution in the One SLATs region.

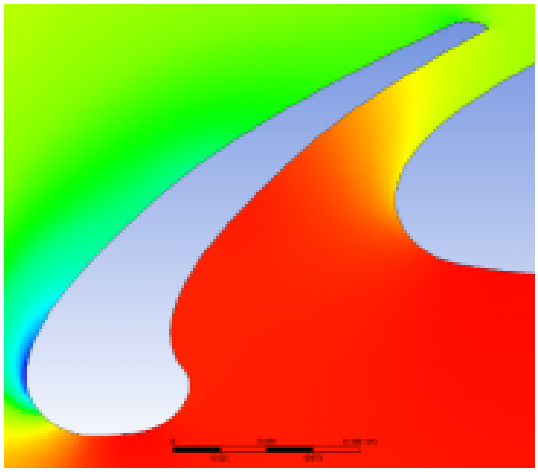

Figure III.20: The contour plots of pressure distribution in the One SLATs region.

We can discern that this configuration has a sharper fall off with higher AOA. Below we have the full result for the 1 slot configuration:

6 Comparison between 1 SLAT and 2 SLAT Configuration:

Although we already exposed the individual result for each configuration, we can only get a full picture by comparing them, the objective of this

Table III.7: One SLATs Simulation Lift and Drag for each AOA.

Alpha	CL	CD	Alpha	CL	CD
20.00	2.095629936	0.067377704	25.25	2.227350949	0.10527657
20.25	2.1069645	0.068762256	25.50	2.229203193	0.107542438
20.50	2.117695297	0.070193883	25.75	2.230183289	0.109896487
20.75	2.127961778	0.071658239	26.00	2.231927426	0.112206914
21.00	2.137671276	0.073161746	26.25	2.233694667	0.114541746
21.25	2.146662191	0.074704901	26.50	2.235865255	0.116850572
21.50	2.154889303	0.076299161	26.75	2.237573092	0.119225294
21.75	2.162824315	0.077937029	27.00	2.238619756	0.121681017
22.00	2.170272283	0.079618565	27.25	2.239173861	0.124203329
22.25	2.17711372	0.081344834	27.50	2.240327498	0.126693587
22.50	2.183580724	0.083256486	27.75	2.241912694	0.129166801
22.75	2.189742866	0.085054821	28.00	2.243806604	0.131633885
23.00	2.195520294	0.086888012	28.25	2.245713277	0.134120769
23.25	2.200899514	0.088774245	28.50	2.246954124	0.136694784
23.50	2.205046477	0.090778817	28.75	2.248837247	0.139228117
23.75	2.210504568	0.092637832	29.00	2.250358888	0.141820931
24.00	2.214200926	0.094635922	29.25	2.252558241	0.144365401
24.25	2.217710625	0.09668446	29.50	2.255257542	0.146877208
24.50	2.220879818	0.098807741	29.75	2.258036869	0.149400098
24.75	2.222770773	0.100865925	30.00	2.259631265	0.152090199
25.00	2.225226401	0.103050085			

thesis is to show the feasibility of a 2 SLOT Airfoil so we start by having a table with 2 configuration side by side and then a chart that do the same.

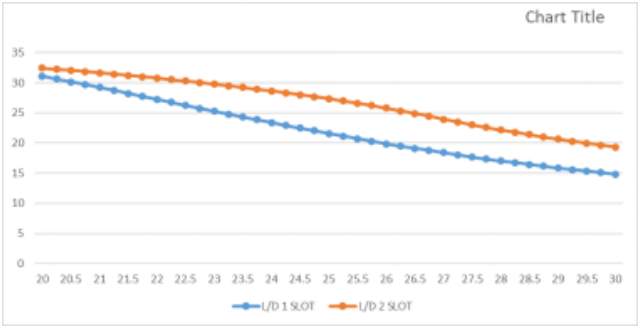

Figure III.21: Chart for the Lift to Drag Coefficient for AOA in SLATs configuration.

We can see that the 2 SLOT do better at all AOA with difference increasing with increased angle, but we can also see that this difference

Table III.8: Result comparison for Two SLATs and One SLATs.

Alpha	CL1/CD1	CL2/CD2	SLOT1-SLOT2	Alpha	CL1/CD1	CL2/CD2	SLOT1-SLOT
20.00	31.102	32.425	1.322	25.25	21.157	26.981	5.824
20.25	30.641	32.242	1.601	25.50	20.728	26.639	5.911
20.50	30.169	32.052	1.883	25.75	20.293	26.249	5.955
20.75	29.696	31.854	2.158	26.00	19.891	25.834	5.943
21.00	29.218	31.653	2.435	26.25	19.501	25.348	5.847
21.25	28.735	31.448	2.713	26.50	19.134	24.905	5.770
21.50	28.242	31.235	2.992	26.75	18.767	24.451	5.683
21.75	27.750	31.008	3.257	27.00	18.397	23.911	5.514
22.00	27.258	30.777	3.518	27.25	18.028	23.532	5.504
22.25	26.764	30.530	3.773	27.50	17.683	23.029	5.346
22.50	26.227	30.290	4.063	27.75	17.356	22.598	5.241
22.75	25.745	30.037	4.292	28.00	17.045	22.169	5.123
23.00	25.268	29.773	4.505	28.25	16.743	21.778	5.034
23.25	24.792	29.502	4.710	28.50	16.437	21.404	4.966
23.50	24.290	29.218	4.928	28.75	16.152	21.011	4.859
23.75	23.861	28.928	5.066	29.00	15.867	20.655	4.787
24.00	23.397	28.627	5.230	29.25	15.603	20.310	4.707
24.25	22.937	28.334	5.397	29.50	15.354	19.987	4.633
24.50	22.476	28.022	5.545	29.75	15.114	19.663	4.549
24.75	22.036	27.692	5.655	30.00	14.857	19.327	4.470
25.00	21.593	27.359	5.766		21.157		

has a critical angle where it stops increasing and start decreasing, that Critical angle is 25.75°. This comparison also shows us the hard fall off for the 1 SLOT that talked about before and put at perspective while this configuration loses 5320° to 30° the 2 SLOT configuration only lose 40At the critical angle of 25.75° there is a 22.6% difference in performance.

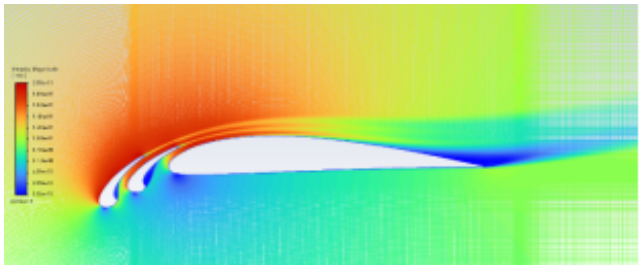

Figure III.22: The contour plots of velocity distribution at 20° in Two SLAT.

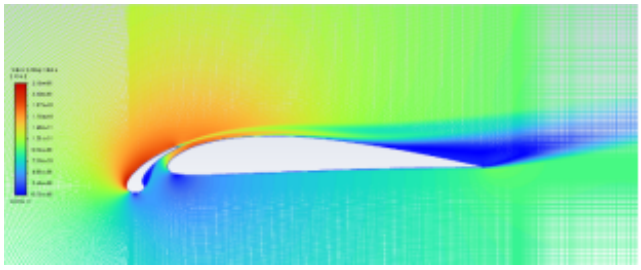

Figure III.23: The contour plots of velocity distribution at 20° in One SLAT

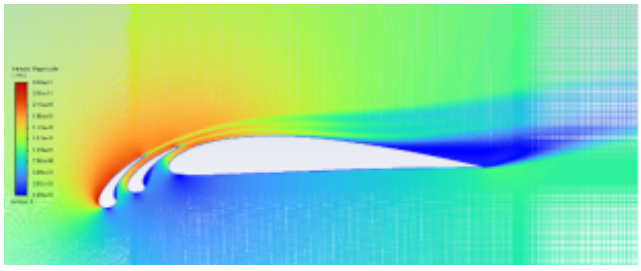

Figure III.24: The contour plots of velocity distribution at 25° in Two SLAT

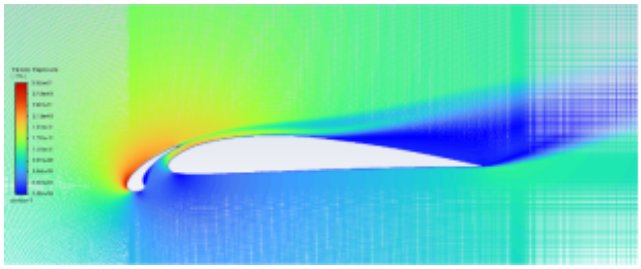

Figure III.25: The contour plots of velocity distribution at 25° in One SLAT

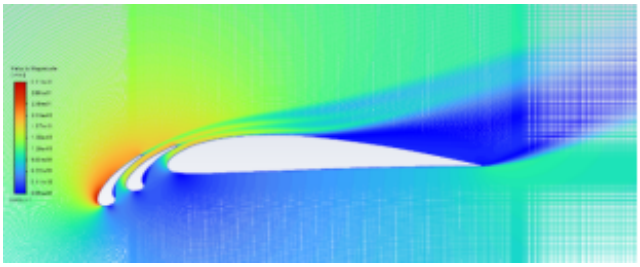

Figure III.26: The contour plots of velocity distribution at 30° in Two SLAT

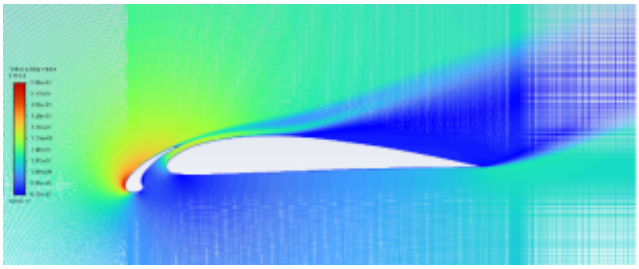

Figure III.27: The contour plots of velocity distribution at 30° in One SLAT

7 Conclusion:

e learned a lot from this number, but graphical representation is the best way to drive a point across so we present 3 visualizations of the velocity for each configuration at 3 different AOA. We can visuals the flow separation and we can see at each given angle the separation takes longer for the 2 SLOT Configuration. We can also better observe the effect unoptimized Tips, we can see that the back flow on the them cause the flow slowdown that reduce the effectiveness of the Leading edges.

General conclusion:

We learned a lot from this number, but graphical representation is the best way to drive a point across so we present 3 visualizations of the velocity for each configuration at 3 different AOA. We can visuals the flow separation and we can see at each given angle the separation takes longer for the 2 SLOT Configuration. We can also better observe the effect unoptimized Tips, we can see that the back flow on the them cause the flow slowdown that reduce the effectiveness of the Leading edges. This thesis focused on the design and simulation of a slat for the USA-35B airfoil to improve its performance at high angles of attack (AOA). Using ANSYS Fluent for 2D simulations, we analyzed the aerodynamic characteristics, specifically the lift coefficient (CL) and drag coefficient (CD), to assess the effectiveness of our slat design. The design process involved a detailed examination of slat geometry and positioning to enhance airflow management around the airfoil. Our primary objective was to delay flow separation and increase the lift-to-drag ratio at high AOA, a critical performance factor for various aeronautical applications. Simulation results demonstrated a significant improvement in the aerodynamic performance of the USA-35B airfoil with the addition of the slat. At high AOA, the slat-equipped airfoil showed higher CL values compared to the baseline configuration, indicating enhanced lift characteristics. Additionally, the CD values were effectively managed, resulting in a better lift-to-drag ratio. These improvements confirm that our slat design successfully delays flow separation, thereby maintaining higher lift and reducing drag penalties at critical operating conditions. Overall, this study underscores the potential of slats in improving airfoil performance, particularly in challenging aerodynamic environments. The findings contribute valuable insights into the design of high-lift devices and their practical applications in aeronautics. Future work could extend these simulations to three-dimensional analyses and explore the effects of different slat configurations to further optimize airfoil

performance. This research paves the way for more efficient and effective designs, enhancing the overall aerodynamic capabilities of aircraft.

General Conclusion

We learned a lot from this number, but graphical representation is the best way to drive a point across so we present 3 visualizations of the velocity for each configuration at 3 different AOA. We can visuals the flow separation and we can see at each given angle the separation takes longer for the 2 SLOT Configuration. We can also better observe the effect unoptimized Tips, we can see that the back flow on the them cause the flow slowdown that reduce the effectiveness of the Leading edges. This thesis focused on the design and simulation of a slat for the USA-35B airfoil to improve its performance at high angles of attack (AOA). Using ANSYS Fluent for 2D simulations, we analyzed the aerodynamic characteristics, specifically the lift coefficient (CL) and drag coefficient (CD), to assess the effectiveness of our slat design. The design process involved a detailed examination of slat geometry and positioning to enhance airflow management around the airfoil. Our primary objective was to delay flow separation and increase the lift-to-drag ratio at high AOA, a critical performance factor for various aeronautical applications. Simulation results demonstrated a significant improvement in the aerodynamic performance of the USA-35B airfoil with the addition of the slat. At high AOA, the slat-equipped airfoil showed higher CL values compared to the baseline configuration, indicating enhanced lift characteristics. Additionally, the CD values were effectively managed, resulting in a better lift-to-drag ratio. These improvements confirm that our slat design successfully delays flow separation, thereby maintaining higher lift and reducing drag penalties at critical operating conditions. Overall, this study underscores the potential of slats in improving airfoil performance, particularly in challenging aerodynamic environments. The findings contribute valuable insights into the design of

high-lift devices and their practical applications in aeronautics. Future work could extend these simulations to three-dimensional analyses and explore the effects of different slat configurations to further optimize airfoil performance. This research paves the way for more efficient and effective designs, enhancing the overall aerodynamic capabilities of aircraft.

References

[1] J. John D. Anderson, *INTRODUCTION TO FLIGHT*, McGraw Hill, 2022.

[2] FAA, *Airplane Flying Handbook (FAA-H-8083-3C)*, [En ligne]. Available: https://www.faa.gov/sites/faa.gov/files/regulations_policies/handbooks_manuals/aviation/airplane_handbook/06_afh_ch5.pdf. [Accès le 04 06 2024].

[3] P. K. Kundu, *Fluid Mechanics (Sixth Edition)*, Academic Press, 2015.

[4] I. L. Imane Khalil, *Computational Fluid Dynamics: An Introduction to Modeling and Applications*, McGraw Hill, 2022.

[5] "Airfoil tools," [En ligne]. Available: http://airfoiltools.com/airfoil/details?airfoil=usa35b-il. [Accès le 04 06 2024].

[6] ANSYS, *ANSYS FLUENT 12.0 User's Guide*, Ansys, 2012.

[7] J. John D. Anderson, *Introduction to Flight*, McGraw Hill, 2022.

[8] "SKYbrary," 04 06 2024. [En ligne]. Available: https://skybrary.aero/articles/angle-attack-aoa.

[9] volupe, "Y+ Compute Grid Spacing online," 04 06 2024. [En ligne]. Available: https://volupe.se/wall-y-calculator-when-meshing-a-geometry-for-cfd-analysis-this-handy-volupe-calculator-computes-the-

[10] A. T. Bahill, "Using the Systems Engineering Process to Explain Baseball's Rising Fastball," INCOSE International Symposium, p. 274, 2003.

[11] R. Krishnamurthy, "The Art and Science of Meshing Airfoil," [En ligne].

Available: https://blog.gridpro.com/the-art-and-science-of-meshing-airfoil/. [Accès le 04 06 2024].

[12] R. Krishnamurthy, “The Art and Science of Meshing Airfoil,” [En ligne]. Available: https://blog.gridpro.com/the-art-and-science-of-meshing-airfoil/. [Accès le 04 06 2024].

[13] NASA, "Turbulence Modeling Resource," [Online]. Available: https://turbmodels.larc.nasa.gov/. [Accessed: 04-Jun-2024].

Abstarct

We will be designing our own leading-edge SLATs for a USA-35B airfoil, the particularity of our designee is the use of 2 retractable SLATs, this designee will be for High angle of attack, we will be testing this system by using ANSYS Fluent to simulate our 2D airflow and perform a iterative correction to our SLATs we will then compare our different result to get a better idea of the efficiency of our system.

keywords: Aerodynamics ,CFD (Computational Fluid Dynamics) ,Fluent ,2D Airfoil ,Leading-edge Slats ,Dual-slat Design, Lift Enhancement ,Flow Separation ;Turbulence Modeling,

مُلخّص

، وتتميز تصميماتنا B-35USA لجناح طائرة من نوع SLATs) (سنقوم بتصميم حواف أمامية رائدة باستخدام حافتين أماميتين قابلتين للسحب. سيكون هذا التصميم مخص أًا للزوايا العالية للهجوم. سنقوم باختبار هذا النظام لمحاكاة تدفق الهواء ثنائي األلبعاد وإجراء تصحيح تكراري لحوافنا األلمامية. ثم Fluent ANSYS باستخدام برنامج سنقارن نتائجنا المختلفة للحصول على فكرة أفضل عن كفاءة نظامنا.

الكلمات المفتاحيّة: الديناميكا الهوائية، الديناميكا الحسابية للسوائل (ثذض)، فلوينت، جناح هوائي ثنائي الأبعاد، أطراف الجناح الأمامية، تصميم جناح ثنائي الأطراف، تحسين الرفع، فصل التدفق، نمذجة الاضطرابات الحركية

Résumé

Nous allons concevoir nos propres becs de bord d'attaque pour un profil aérodynamique USA-35B. La particularité de notre conception réside dans l'utilisation de deux becs rétractables. Cette conception sera destinée à des angles d'attaque élevés. Nous testerons ce système en utilisant ANSYS Fluent pour simuler notre écoulement d'air en 2D et effectuer une correction itérative de nos becs. Nous comparerons ensuite nos différents résultats pour obtenir une meilleure idée de l'efficacité de notre système.

mots-clés: Aérodynamique, CFD (Dynamique des Fluides Numérique), Fluent, Profil 2D, Volets de bord d'attaque, Conception à double volet, Amélioration de la portance, Séparation des écoulements, Modélisation de la turbulence.